Light Rays in the Gravitational Field of Rotating Disks of Dust in General Relativity

Thesis

to achieve the academic title

doctor rerum naturalium (Dr. rer. nat.)

Presented to the Board of the Physical Astronomy Faculty

of the Friedrich Schiller University Jena

by Declan Moran BSc. ,

born 19 July 1972 in Ballinasloe

Referees:

1. Prof. Dr. G. Neugebauer

2. Prof. Dr. H. Ruder

3. Prof. Dr. T. Henning

Date of Exam (Rigorosum): 19-6-2000

Date of Defence of Thesis: 29-6-2000

Contents

1 Introduction **3**

2 The Rotating Disk Solutions **7**

2.1 The Neugebauer-Meinel Solution 7

2.1.1 The Geodesic Equations 14

2.1.2 The Killing Vectors and Conserved Quantities 15

2.2 The Ansorg-Meinel Solution 16

3 Visualisation of Rotating Disks **20**

3.1 Overview 20

3.2 Plane Projection Surface 23

3.2.1 Redshift 28

3.2.2 Special Relativistic Image Distortion 32

3.3 Spherical Projection Surface 36

4 The Deflection of Light Rays by Rotating Disks **43**

4.1 Analytical Approximation for Rigidly Rotating Disks 44

4.1.1 The Kopeikin-Schäfer Lorentz Covariant Theory of Light Propagation 44

4.1.2 The Deflection Angle 47

4.2 Numerical investigation of highly relativistic Rotating Disks 50

5 The Lensing Nature of Rigidly Rotating Dust Disks **56**

5.1 Caustic Surfaces and Standard Lensing Theory 56

5.2 Numerical Studies of the Caustic Structure of the Disk 66

5.2.1 Caustics for an arbitrarily located Observer 66

5.2.2 Caustics for an observer located on the Symmetry Axis 72

6 Summary and Conclusion **77**

A The Function $V_0(\mu)$ **79**

B Observed Gravitational Lensing Phenomena **80**

1 Introduction

In their quest to understand the world in which we live and its origins scientists have long contemplated the universe as a whole. At the cosmological level however, Newtonian physics is no longer sufficient to describe nature, but rather one has recourse to use Einstein's theory of general relativity. To this end scientists study light and other electromagnetic radiation[1] reaching us from distant parts of space. This radiation contains valuable information which is a complex combination of the properties of not only the source that emitted it, but also each of the objects under whose influence the ray passed on its way to our telescopes. To decipher this information one needs a good understanding of these influences, one of the most important of which is the gravitational fields of celestial bodies, in particular galaxies, located between us and the light sources. Galaxies, such as our own Milky Way and NGC 4414 (see figure 1), are collections of stars held together by their own gravitational field, and constitute one of the fundamental building blocks of the Cosmos.

In 1995 Neugebauer and Meinel [1] succeeded in finding the first global, analytical solution of Einstein's's equations of general relativity for an extended body. The Neugebauer-Meinel solution describes the gravitation field of a rigidly rotating pressure free ideal fluid disk. This so-called rigidly rotating disk of 'dust' can be used to physically model galaxies or galaxy clusters, which to a very good first approximation are rotating disks. This solution can be shown to be the universal limit of rigidly rotating perfect fluid configurations as $p/\epsilon \to 0$ (where p is the pressure and ϵ the mass-energy density) In 1999 Meinel and Ansorg [2] generalised the Neugebauer-Meinel solution to construct a family of solutions that describe differentially rotating disks of dust.

Prompted by the astrophysical motivation described above, the purpose of this thesis is to use these solutions to investigate the influence of a strongly gravitating rotating disk of dust on the propagation of light rays in their vicinity.[2] A striking consequence of Einstein's

[1] In the near future it is hoped that gravitational radiation will also be able to be used to serve the same purpose

[2] The results are valid of course, for any form of electromagnetic radiation.

theory is that light in general, no longer travels in the simple straight lines predicted by Newtonian theory[3]. Instead photon trajectories trace out null geodesics in the curved spacetime continuum, which is warped by the gravitating bodies it contains. In such a spacetime these geodesics are the shortest[4] possible paths on the trajectory, just as in the flat space of Newtonian theory straight lines are the shortest paths between points on the lines.[5] This bending of light rays has important repercussions for astronomers. Such effects are the topics of the following chapters which discuss them from three different points of view.

Chapter 2 focuses on the visualisation of rotating disks as they appear to an observer. Since light rays emitted by objects (including the gravitating object itself) which undergo the deflective influences of a gravitating body, in general appear to an observer to come from a different direction, the light source can appear highly distorted and shifted from its true position. Many striking examples of such distortion of images have been catalogued by astronomers in their observations of the night sky. One particularly interesting aspect of this behaviour is the fact that under appropriate conditions one can for example simultaneously see the top and bottom of the disk, an occurrence which in the rectilinear light propagation of classical physics would be completely impossible.

Chapter 3 concentrates on the deflection of individual light rays and how the deflection angle depends on the parameters of the disk and the ingoing light ray. In fact, one of the most convincing evidences for Einstein's theory was the first observation of such a deflection during a solar eclipse by Eddington on his famous expedition in 1919. A post-Minkowskian expression is derived using the results of Kopeikin-Schäfer [10] and the deflection angle proves to be a very illustrative comparison of rigidly and differentially rotating disks.

[3]or indeed special relativity, although special relativity does itself lead to a distortion of the visual appearance of objects when source and observer are moving relative to one another with high speeds. See [7] and [8] for very interesting treatments.

[4]more accurately, the maximal

[5]Surprisingly Newtonian spacetime is in fact curved. It is interesting that Einstein flattened spacetime with the introduction of the Minkowski manifold, and later incorporated gravity into his theory by allowing spacetime to curve under its influence.

The theme of the final chapter is the lensing properties of the rotating disks of dust. The topic gravitational lensing has become an increasingly important and active area of research in recent years, particularly since the discovery of the first gravitational lens by Walsh, Carswell and Weymann [13] in 1979. Lensing theory is not only an interesting consequence of Einstein's theory but also offers the prospect of being a considerable help to astronomers in more accurately determining many of the constants of the universe including Hubble's constant. These natural telescopes allow us to look much further back in time and space than would otherwise be possible. The distinct lack of physically relevant solutions to Einstein's equations means that lensing theorists generally need to rely heavily on approximations and other simplifications. Thanks to the explicit solution it is possible to probe the lensing structure of the rotating disk well beyond the usual weak field approximations and small deflection angle assumptions of standard lensing theory.

In the following chapters, figures 2-6 and 50 are taken from [29], figures 7,8 and 9 are from [2], and 38, 39 are from [23]. Figure 1 and the two images (figures 51 and 52) in appendix B, are the work of W. Freedman, J. Hewitt and F. D. Macchetto respectively, as stated in the corresponding captions. Shown in figures 10, 11, 18, 23, 28, 34, 35, 36, 37, 43, and 44 are sketches intended to illustrate concepts or numerical methods presented in the text. All other figures are the direct results of numerical computation.

Figure 1: This image of the majestic spiral galaxy NGC 4414, located 60 million light years from the earth was recorded in 1995 by Wendy Freedman et al. with the Hubble Space Telescope. The gravitational fields of such galaxies are a major influence on the lightrays reaching the earth from the distant corners of the universe. A complete and consistent study of the effects of the gravitational fields produced by massive astrophysical bodies requires recourse to Einstein's theory of general relativity and in particular the solutions for rotating disks of dust introduced in chapter 2.

2 The Rotating Disk Solutions

2.1 The Neugebauer-Meinel Solution

The metric for an axisymmetric stationary and asymptotically flat spacetime, in Weyl-Lewis-Papapetrou-coordinates $(\rho, \zeta, \varphi, t)$ is:

$$(g_{ij}) = \begin{pmatrix} e^{2(k-U)} & 0 & 0 & 0 \\ 0 & e^{2(k-U)} & 0 & 0 \\ 0 & 0 & -a^2 e^{2U} + \rho^2 e^{-2U} & -a e^{2U} \\ 0 & 0 & -a e^{2U} & -e^{2U} \end{pmatrix} \tag{1}$$

yielding the line element[6]

$$ds^2 = e^{-2U}[e^{2k}(d\rho^2 + d\zeta^2) + \rho^2 d\varphi^2] - e^{2U}(dt + a\, d\varphi)^2\,. \tag{2}$$

With this metric, the vacuum Einstein equations are equivalent to the Ernst equation

$$(\Re f)\, \triangle f = (\nabla f)^2\,, \tag{3}$$

$$\triangle = \frac{\partial^2}{\partial\rho^2} + \frac{1}{\rho}\frac{\partial}{\partial\rho} + \frac{\partial^2}{\partial\zeta^2}, \qquad \nabla = \left(\frac{\partial}{\partial\rho}, \frac{\partial}{\partial\zeta}\right),$$

where the Ernst potential f is given by

$$f = e^{2U} + \mathrm{i}\, b \tag{4}$$

and

$$b_{,\zeta} = \frac{e^{4U}}{\rho}\, a_{,\rho}, \quad b_{,\rho} = -\frac{e^{4U}}{\rho}\, a_{,\zeta}. \tag{5}$$

$$k_{,\rho} = \rho\,[\, U_{,\rho}^2 - U_{,\zeta}^2 + \frac{1}{4}\, e^{-4U}(b_{,\rho}^2 - b_{,\zeta}^2)\,], \quad k_{,\zeta} = 2\rho\,[\, U_{,\rho}\, U_{,\zeta} + \frac{1}{4}\, e^{-4U}(b_{,\rho} - b_{,\zeta})\,] \tag{6}$$

[6] note that in the units used the speed of light and Newton's gravitational constant are equal to unity: c=G=1.

The axisymmetry and stationarity of the spacetime admits two Killing vectors ξ^i and η^i respectively[7]

$$\xi^i = \delta^i_t, \quad \xi^i\xi_i < 0 \quad \text{(stationarity)} \tag{7}$$

$$\eta^i = \delta^i_t, \quad \eta^i\eta_i < 0 \quad \text{(axisymmetry)} \tag{8}$$

where δ^i_j is the usual Kronecker delta. In the chosen coordinate system $\xi^i = (0, 0, 0, 1)$ and $\eta^i = (0, 0, 1, 0)$

The 4 velocity of the disk 'particles' can be expressed as

$$u^i = e^{-V}(\xi^i + \Omega\eta^i), \quad \text{with} \quad u^iu_i = -1 \tag{9}$$

where Ω is the angular velocity and in the case of the rigidly rotating disk, is constant. The energy momentum tensor for a pressure free perfect fluid is

$$T^{ik} = \epsilon u^i u^k \tag{10}$$

which for the disk of dust can be expressed

$$T^{ik} = \sigma_p(\rho)e^{U-k}\delta(\zeta)u^iu^k \tag{11}$$

where ϵ and σ_p represent the energy-density and the invariant (proper) surface mass-density, respectively, and δ is the usual Dirac delta-distribution. Conservation of energy-momentum requires the vanishing of the covariant divergence

$$T^{ij}{}_{;j} = 0 \tag{12}$$

Neugebauer and Meinel [1] succeeded in solving the Ernst equation for the case of a rigidly rotating (Ω =const) pressure free perfect fluid ('dust') disk, using a technique from soliton physics called the 'inverse scattering method'. Their solution depends on two parameters : the radius ρ_0, and the angular velocity Ω, of the disk. In the dimensionless coordinates $(\rho/\rho_0, \zeta/\zeta_0, \phi, t)$ one may regard the Ernst potential as depending on another parameter μ,

$$\mu = 2\Omega^2\rho_0^2 e^{-2V_0(\mu)} \tag{13}$$

[7]Here, as elsewhere in the text (unless stated otherwise), the usual notation convention applies: Repeated indices in a single term are to be summed over from $1 \to 4$. A comma denotes partial differentiation, and a dot above the variable represents partial differentiation w.r.t. the affine parameter τ. Indices are raised and lowered via the metric.

which is a useful measure of how strongly relativistic the disk is. This parameter can take values in the range: $\mu \in (0, \mu_0)$ where $\mu = 0$ yields Minkowski spacetime and $\mu = \mu_0 (\simeq 4.62...)$ is the ultrarelativistic limit corresponding to an extreme Kerr black hole (see figure 5). The function $V_0(\mu)$ appearing in the implicit equation 13 can be expressed using the Weierstraß function.[8] The normalised surface mass density σ_p/Ω is plotted in figure 2 as a function of the dimensionless radial coordinate ρ/ρ_0, for several values of μ. An interesting feature of this diagram is the appearance of a maximum toward the rim of the disk when $\mu \simeq 1.6$, a purely relativistic feature which is not exhibited by the classical analogue, the MacLaurin disk.

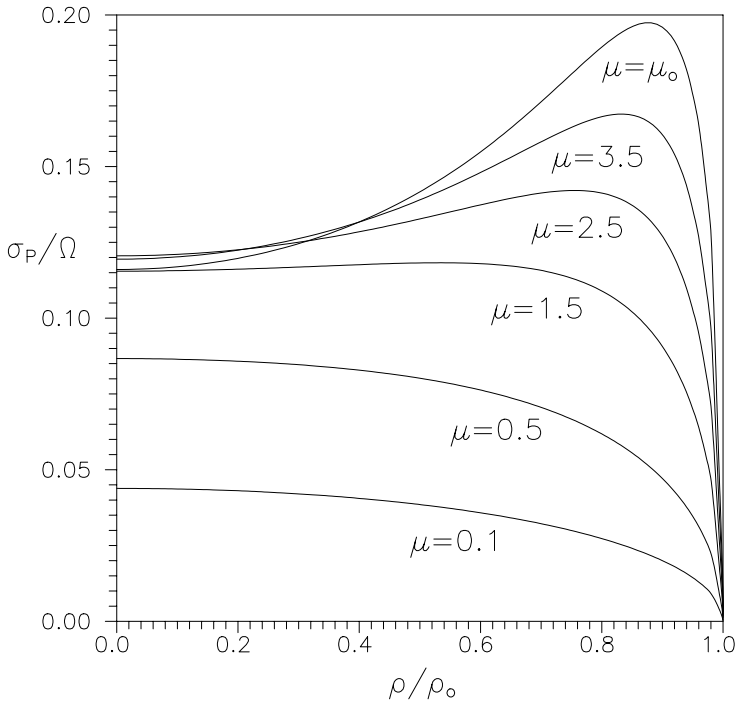

Figure 2: The normalised surface rest mass density as a function of the normalised radial coordinate.

Using Komar integrals one can obtain expressions for the mass and angular momentum of the disk:

[8] see Appendix A for details.

$$M_0 = \int_\Sigma \epsilon\sqrt{-g}u^4 d^4x = 2\pi e^{-V_0} \int_0^{\rho_0} \sigma_p e^{k-U} \rho d\rho, \tag{14}$$

$$M = 2\int_\Sigma (T_{ab} - \frac{1}{2} t g_{ab}) n^a \xi^b dV = 2\pi \int_0^{\rho_0} \sigma_p + 4\pi\Omega e^{-V0} \int_0^{\rho_0} \sigma_p e^{k-U} u^i \eta_i \rho d\rho \tag{15}$$

$$J = -\int_\Sigma T_{ab} n^a \eta^b dV = 2\pi e^{-V_0} \int_0^{\rho_0} \sigma_p u^i \eta_i \rho d\rho \tag{16}$$

Where M_0 is the total rest mass of the disk, M the total mass, J the total angular momentum, $T = g_{ij}T^{ij}$, and Σ is the spacelike hypersurface t=constant with the future pointing normal vector n^a. It is also possible to consider (M,J) to be the two independent parameters of the metric rather than (Ω, ρ_0). Plots of these quantities as a function of the relativistic parameter μ can be seen in figure 3

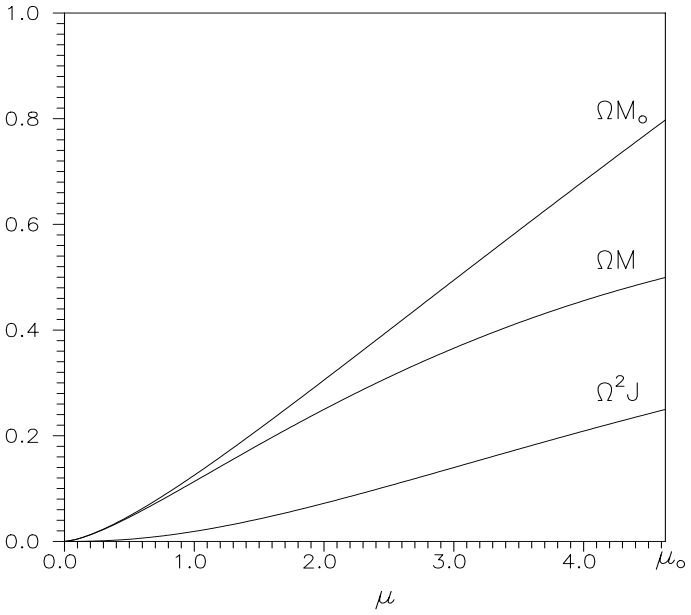

Figure 3: The quantities ΩM_0, ΩM, $\Omega^2 J$ as a function of μ.

Another useful measure of the relativistic strength of the disk is the quantity M^2/J (which will be used in subsequent chapters to relate rigidly and differentially rotating disks). This quantity and the relative binding energy are both monotonically increasing functions of the relativistic parameter μ (see figure 4).

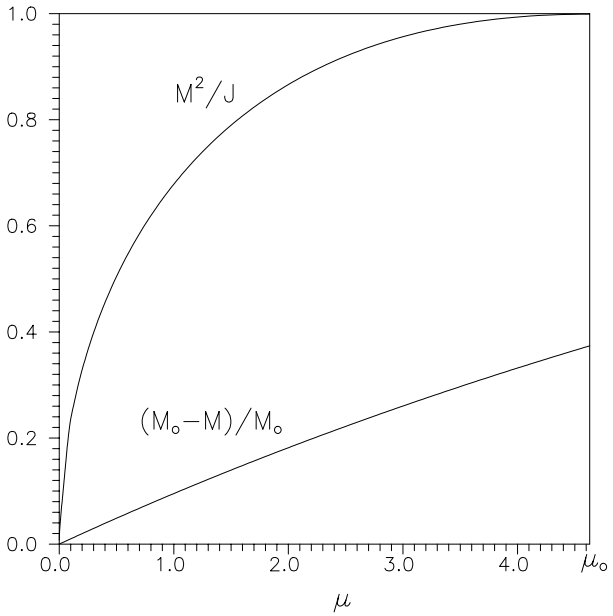

Figure 4: The quantities M^2/J, and the relative binding energy as a function of μ.

In the limit as $\mu \to \mu_0$, $\rho_0 \to 0$ (for $\rho^2 + \zeta^2 \neq 0$) the solution approaches the extreme Kerr solution (see figure 5)

$$M = \frac{1}{2\Omega} \ , \ J = \frac{1}{4\Omega^2}$$

As is typical for relativistically rotating bodies, at sufficiently large values of the relativistic parameter μ an ergoregion appears (see figure 6) inside of which all massive (test) bodies are dragged in the direction of rotation of the disk.[9] This ergoregion inside of which the Killing vector associated with the stationarity of the spacetime ξ^i, becomes spacelike is topologically equivalent to a torus.

[9]see also [14] for an interesting discussion of the dragging effects and the ergoregion.

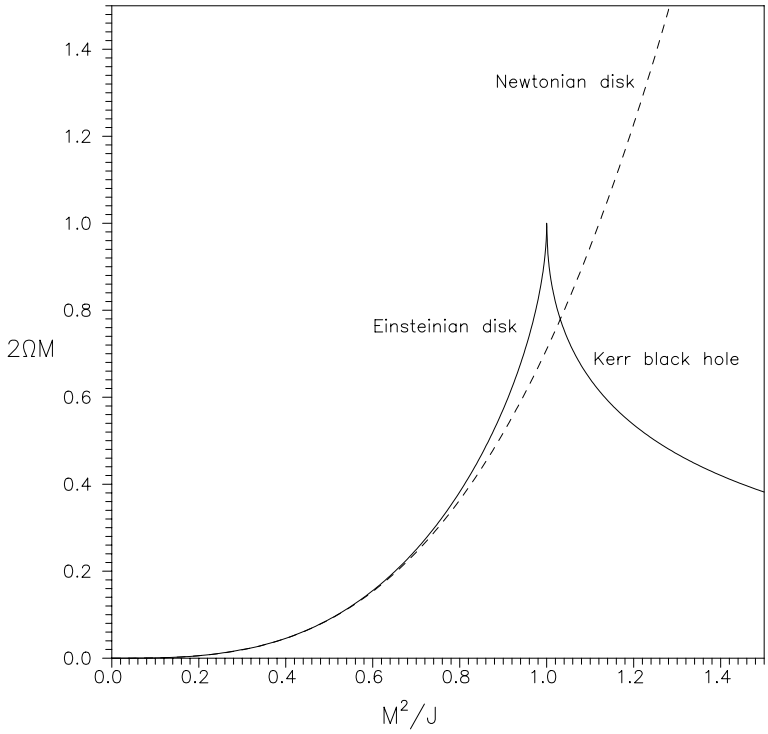

Figure 5: The transition to the extreme Kerr solution as $M^2/J \to 1$.

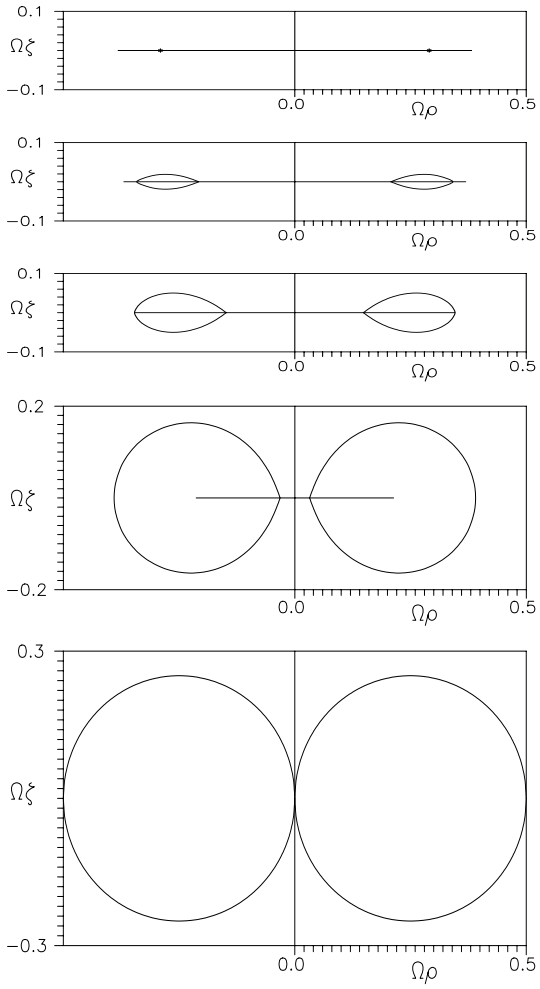

Figure 6: The appearance of the ergoregion at $\mu \simeq 1.68$ and its evolution as a function of μ.

2.1.1 The Geodesic Equations

In order to calculate the photon trajectories it is necessary to solve the corresponding geodesic equations:

$$\ddot{x}^i + \Gamma^i_{jk}\dot{x}^j\dot{x}^k = 0 \tag{17}$$

subject to the normalisation

$$\dot{x}^i\dot{x}_i = 0 \tag{18}$$

where the Christoffel symbols Γ^i_{jk} are given by

$$\Gamma^i_{jk} = \frac{1}{2}g^{id}(g_{dj,k} + g_{kd,k} - g_{dj,k}) \tag{19}$$

The metric g_{ij} has the form given in equation 1.

This second order system of differential equations cannot be solved explicitly due to the complexity of the metric, but rather one has recourse to use numerical methods which execute a piecewise integration of the equation system, resulting in a polygon approximation to the trajectory of the light ray. Solution requires prescribing eight initial conditions: the four starting spacetime coordinates x^i and their initial derivatives $\dot{x}^i$ w.r.t. the affine parameter τ. The first four of these initial conditions are fixed by the observer's position in spacetime (the centre of the disk being always located at the origin of the coordinate system, and the value chosen for the initial time coordinate of the observer will have no effect on the path of the resulting light ray), the next three by the parameters of the light ray: two angles specifying the spatial direction of emission, and an additional parameter which can be considered to correspond to the frequency of the emitted photon.[10] The eighth and final initial condition is satisfied by the requirement equation 18 which encodes into the solution that the particles in question have zero rest mass, and as such travel at the speed of light.

[10] In general this can be considered to correspond to the momentum of the emitted particle which could in turn be associated with the speed of a timelike particle or the frequency of a lightlike one which must always travel at the speed of light ..c=1 here.. remember the same geodesic equations determine the path of timelike particles with the proviso $\dot{x}^i\dot{x}_i = -1$).

The solution of these equations numerically via a 5th order Runge-Kutta method was implemented by Ansorg [3] in a computer subprogram of which extensive use was made in the following chapters. In this implementation a Chebychev approximation of the metric in elliptical coordinates was used to speed up the calculation time for the geodesics.

2.1.2 The Killing Vectors and Conserved Quantities

It can be shown[11] that associated with each Killing vector field there is a conserved quantity along each geodesic in the spacetime. Thus if χ^i is a Killing vector field i.e. a vector field satisfying the Killing equation

$$\nabla_i \chi_j + \nabla_j \chi_i = 0$$

then for each geodesic with tangent four vector u^i the quantity

$$\chi^i u_i = const \tag{20}$$

is conserved along the geodesic. Thus in the Neugebauer Meinel solution one expects 2 conserved quantities along any geodesic corresponding to the 2 Killing vector fields ξ^i and η^i. These two conserved quantities, L and E are a consequence of the axial symmetry and stationarity of the spacetime. Explicit expressions can be calculated for these quantities in Weyl-Lewis-Papapetrou coordinates by combining equations 20 and 1 and remembering that in these coordinates the two Killing vectors are given by $\xi = (0, 0, 1, 0)$ and $\eta = (0, 0, 0, 1)$.

Thus $u^i g_{i3} = u^3 g_{33} + u^4 g_{34}$ and $u^i g_{i4} = u^3 g_{34} + u^4 g_{44}$, yielding the expressions:

$$E = g_{34}\dot{\phi} + g_{44}\dot{t} \tag{21}$$

$$L = g_{33}\dot{\phi} + g_{34}\dot{t} \tag{22}$$

for the conserved quantities along any geodesic in the Neugebauer-Meinel spacetime.

[11] see for example [11] section C.3.

In a Hamiltonian treatment of the geodesic equations Ansorg [3] defined a quantity h by the equation

$$h = \frac{1}{2}[1 - \frac{(L^2 g_{44} + 2LEg_{34} + E^2 g_{33})}{\rho^2}] \tag{23}$$

and showed that for geodesics h cannot be positive

$$h(\rho, \zeta, L, E) \leq 0 \tag{24}$$

Thus one can make some general statements about the possible regions of spacetime which cannot be reached by photons, which are analogous to the constraints placed by conservation of energy and momentum in classical mechanics. This analogy leads one to call E the energy of the photon and L its angular momentum. Defining $r = \sqrt{\rho^2 + \zeta^2}$ and taking the appropriate limits in equation 23 one can show that $r \to \infty$ is not allowed for photons with $E^2 < 1$. Only when the energy of the photon is such that $E^2 \geq 1$ can it escape to spatial infinity. Similar considerations of the angular momentum L show lead to the conclusion that only photons with zero angular momentum $L = 0$ can cross the axis of symmetry of the disk.

2.2 The Ansorg-Meinel Solution

In 1999 Meinel and Ansorg [2] generalised the Neugebauer-Meinel solution to allow disks with non-constant angular velocity. Formally the metric, Ernst potential and Energy-Momentum tensor have the same structure (see equations 1, 4, 10), and there are also two Killing vector fields and associated conserved quantities analogous to those in equations 21 and 22. But whereas the Neugebauer-Meinel solution had two independent parameters, now there are three. (It is possible to consider the extra parameter as corresponding to the $\Omega(\rho)$ profile which is now an extra degree of freedom). These three parameters are embodied in (the real and imaginary parts of) the complex parameter X_1, and as before, the radius ρ_0 of the disk.[12]

[12]In order to calculate the Ernst potential the numerical evaluation of a certain 'jump' function was necessary. The accuracy of this evaluation can however in principle be increased indefinitely, so that for the purpose of the investigation of the behaviour of light rays, or other such phenomena, this is no cause for concern.

The parameter space of X_1^2 can be seen in figure 7 together with the characteristic properties of the corresponding solutions. One notes in particular that one recovers the rigidly rotating disks with $\mu = 1/\Im(X_1^2)$ when $\Re(X_1^2) = -1$. Disks with a value of $\Re(X_1^2)$ greater/less than -1 have a decreasing/increasing density profile respectively.

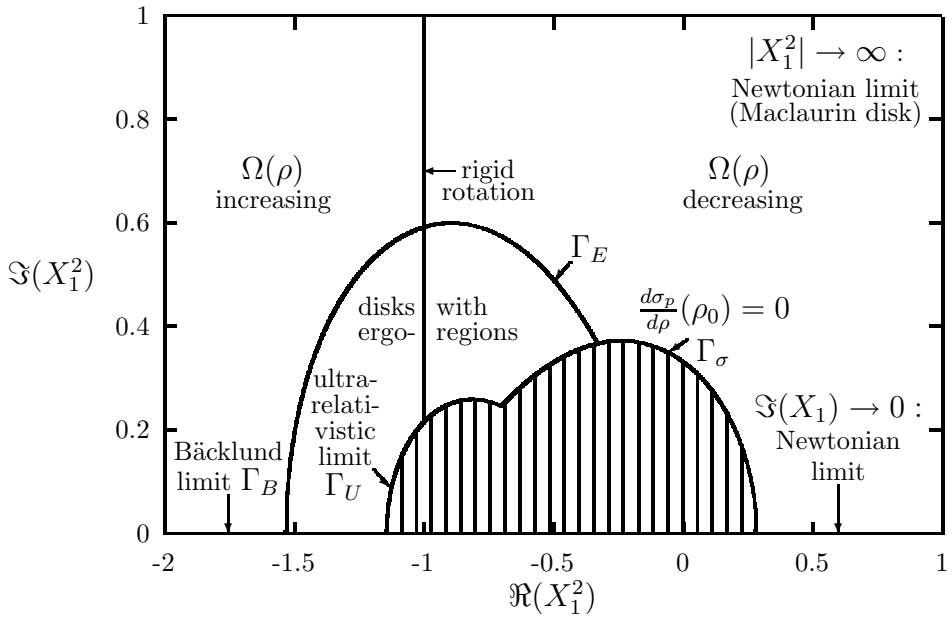

Figure 7: The parameter space of X_1^2 with the physical characteristics of the corresponding solutions, which are to be found only outside the hatched region.

Figure 8 illustrates the behaviour of the surface mass density and angular velocity of a selection of disks. Formally identically as for the Neugebauer-Meinel disk, one can define the mass and angular momentum of the Meinel-Ansorg disks (see equations 14, 15 and 16). A useful possible means of bench marking disks with different density profiles is through the value of M^2/J. Disks with equal values of M^2/J can be considered 'equally relativistic' in a certain sense, where $M^2/J \to 0$ characterises Newtonian disks and $M^2/J \to 1$ extremely relativistic ones. Use will be made of this criterion in subsequent chapters when contrasts are made between rigidly rotating disks and differentially rotating counterparts which are considered 'comparable' in this sense. A contour plot of M^2/J over the parameter space of X_1^2 can be seen in figure 9.

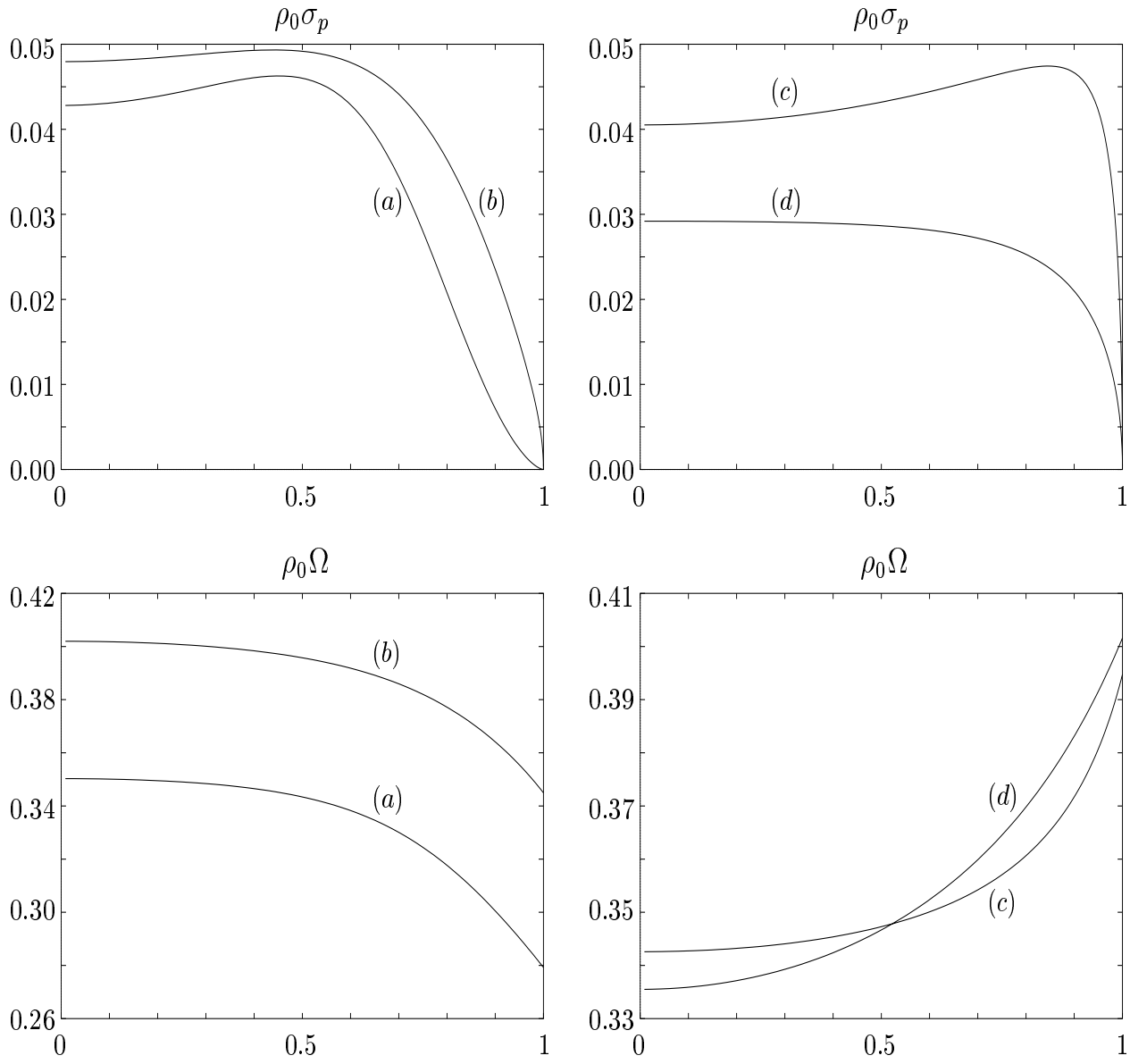

Figure 8: The dimensionless quantities $\rho_0\sigma_p$, and $\rho_0\Omega$ as a function of the normalised radial coordinate ρ/ρ_0. The curves plotted correspond to parameter values given by: (a) $X_1^2 = -1/2 + i/3$, (b) $X_1^2 = -2/3 + i/2$, (c) $X_1^2 = -3/2 + i/5$, (d) $X_1^2 = -4$.

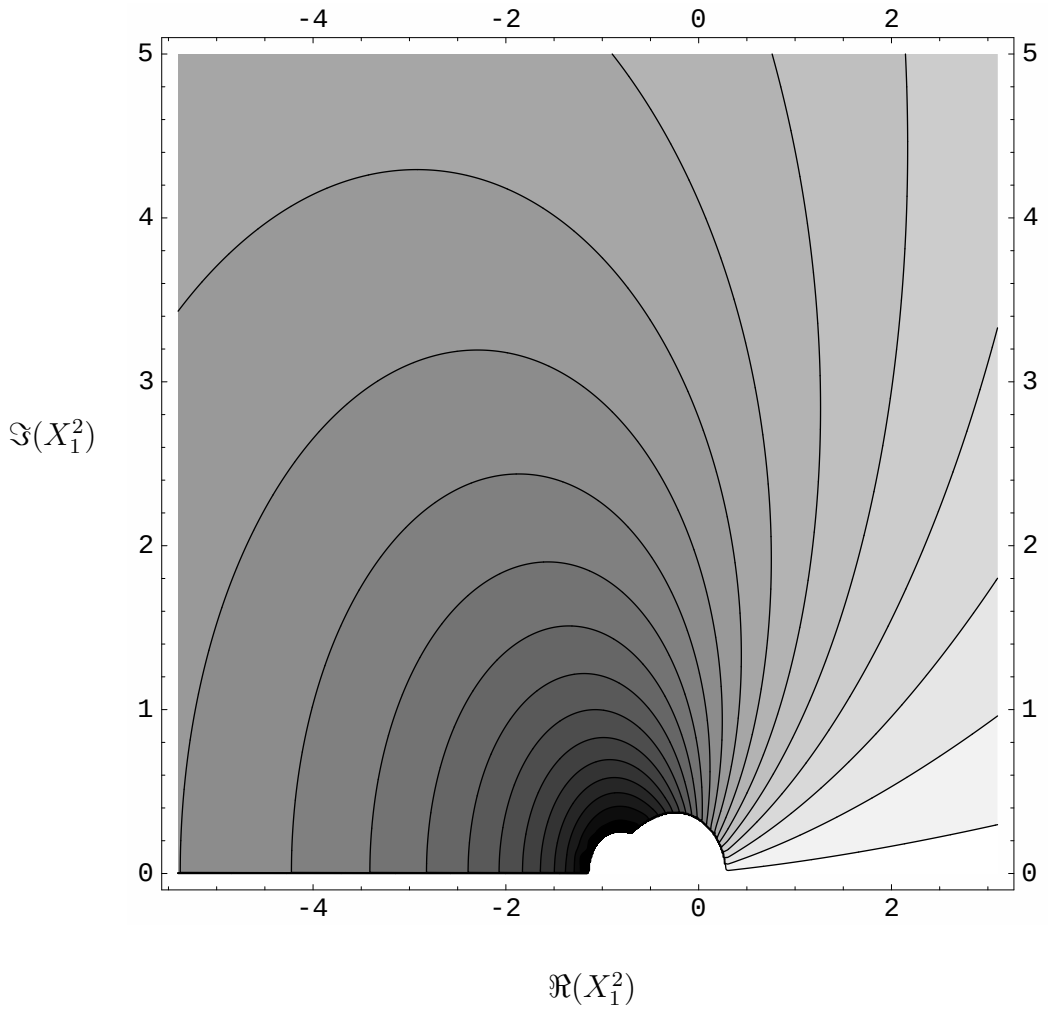

Figure 9: A contour plot of M^2/J .The isophotes represent equal values of M^2/J ranging from 0 (brightest) $\rightarrow$ 1 (darkest), with neighbouring isophotes differing by 1/20. As in figure 8, $\Re(X_1^2) = -1$ corresponds to rigidly rotating disks with $\Im(X_1^2) = 1/\mu$.

3 Visualisation of Rotating Disks

3.1 Overview

The visual appearance of an object can be greatly influenced by the presence of a gravitating body located (roughly) between the object and the observer. A gravitational field deflects light rays from what would otherwise be a rectilinear path with the effect that those reaching the eye of an observer[13] appear to come from a direction other than that from which they were actually emitted. The same also applies to the image of the gravitating body itself. A light emitting[14] disk considered to isotropically emit photons will in general warp the spacetime through which the photons travel so that the photons, following geodesics in this curved spacetime, will no longer propagate isotropically or rectilinearly.

A method known as 'ray-casting' can be applied to calculate the image as seen by an observer of such a disk. In this scheme light rays are followed from the observer's eye, which is taken to be a very small (but still of finite size) two dimensional surface,[15] back towards the disk. Those rays which strike the surface of the disk are those contributing to the visual image. Much pioneering work has been done in recent years on visualisation in relativity by scientists such as H. Ruder et al. using methods of this kind, and the reader is referred to the very illustrative and interesting presentations which can be found in [4], [5], [6], [7] and [8] and other references therein.

Consider the situation illustrated in figure 10 where such a ray is depicted. The disk emits a light ray from the point A, which follows the solid curve to the observer's eye.

[13] or any other visual detector such as a telescope or photographic plate

[14] This is also true if the gravitating object is not the source of the light but rather reflects light incident upon it from a light source located somewhere else. For the purpose of this discussion however, this and other subtleties such as the reflection coefficient of the surface of the body will not be considered since they do not probe the effects of the gravitational field any further, which is the main aim here.

[15] typically a section of a 2-sphere, the solid angle made with the centre of the sphere corresponding to the angular field of view of the observer, humans having an angular field of view less than 180 °

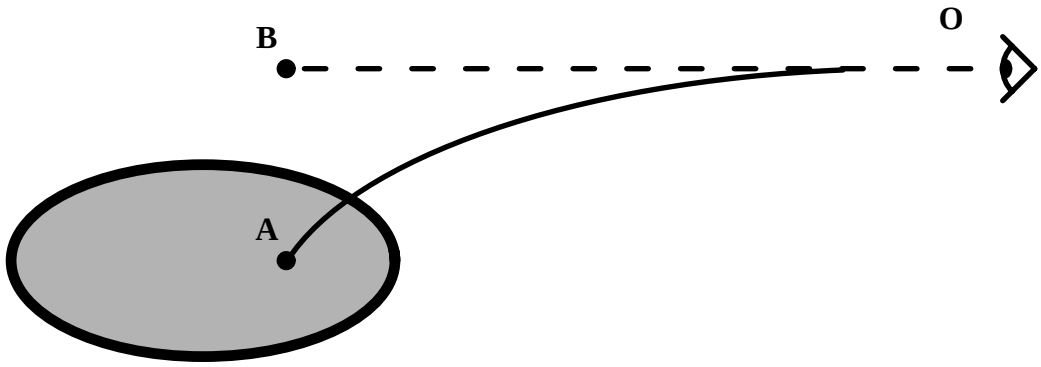

Figure 10: A point A on the disk emits a photon which travels along the solid line reaching the observer O. To the observer however the light ray seems to have travelled along the dotted line which is the tangent to the true path at the eye of the observer, putting the observer under the impression that the emission point was B. (To be more precise the observer cannot in general tell where along the dotted line the photon appeared to be emitted from. Other visual aids, such as the binocular vision of humans, are necessary to decipher this).

The observer lacking the knowledge of what curve the photon really travelled, interprets this as best he can, namely as straight line extrapolated tangent to the incident ray back to the point B, which he then regards as the emission point. In effect the image of the point A on the disk is the point B, from the observer's point of view (literally!). The same applies to all other rays emitted from the disk and reaching the observer. Thus a plausible way to construct the image of the whole disk would therefore be to consider each point on the disk (in fact each small surface element, the size of which would determine the resolution of the final picture) in turn and to calculate the trajectory of each (again in practice this would mean many light rays distributed evenly throughout the spectrum of emission angles) photon that the point could emit. One would then check whether the light ray in question intersects the surface representing the observer's eye or not. If so, the ray contributes to the image and the point of emission and angle of incidence are both saved for later processing. If not, the ray does not contribute to the image and should be discarded.

This procedure although yielding the desired result, is however less efficient than the above mentioned method using ray-casting which in practice is preferred. Here one relies

on the reversibility of light rays (by which is meant that if a light ray can travel the curved line in figure 10 from A to O then a light ray could also travel along the same curve but in the opposite direction, namely from O to A[16]) to achieve the same goal. Instead of checking all emitted rays from each point on the disk for intersection with the observer's eye, one checks all rays that could be 'emitted' from the location of the observers eye for intersection with *any* point on the disk. Thus in effect one has to consider only one point of emission and each ray has a significantly better chance of striking the 'target' (the disk is significantly bigger than the eye). The resolution of the resulting image is determined by the angular separation of the rays traced back from the observer.[17]

In order to implement the above scheme based on ray-casting one also needs to choose a suitable projection surface. This projection surface is somewhat arbitrary and serves the function of an abstract canvas on which one 'paints' the image seen by the observer. Once all contributing light rays have been calculated, one extracts the relevant information necessary to construct the image, namely the angle of emission from the observer and the point struck on the disk. The latter is strictly speaking only necessary when one wishes to visualise the disk with a pattern such as alternating dark and white tiles as will be the case in most of the figures below. The inclusion of such a pattern enhances the depiction by conveying extra visual information about the 'internal' distortion of the image of the disk. One then proceeds to extrapolate from the observer along the tangent to the emitted ray back to an intersection point (if any...extrapolated tangents which fail to strike the projection surface correspond to image points lying outside the observers field of view. Plane projection surfaces clearly allow a maximum field of view of slightly less than 180°... a 180° field of view would necessitate an infinitely large plane projection surface. The possibility, which will be explored later in the chapter, exists however to use a projection

[16]In Newtonian physics this is clear since the light rays are just straight lines, and in Einstein's theory this can be guaranteed if the geodesic equations are invariant with respect to a negation of the time coordinate, a condition fulfilled by the stationarity of the metric in the Neugebauer-Meinel solution.

[17]Note that one could also allow the possibility of translucent disks by incorporating a non-zero probability that light rays extended back from the observer's eye and which hit the disk, pass through. These rays would then not contribute to the image. This probability distribution would be a manifestation of the type of material composing the disk. As for the surface properties, such deliberations will not be dwelt upon in this chapter, being considered irrelevant from the point of view of the gravitational field which is insensitive to the type of matter constituting the disk.

surface which is not planar but for example spherical. This spherical projection surface could be considered to be the 'sky' of the observer.) with the projection surface which becomes a point to be painted on the canvas. Advancing in this manner for all rays under consideration one constructs a pattern on the projection surface. One then can justifiably assert that the pattern so mapped onto the projection surface would appear to the observer, were both embedded in 'everyday' Newtonian spacetime, exactly as does the disk, both it and observer being embedded in the curved four dimensional spacetime moulded by the gravitational field of the disk.

3.2 Plane Projection Surface

The most intuitive, even if not the most effective, projection surface is a section of a plane. For relatively small angular image sizes (say $\lesssim 60°$), this is a very satisfactory option. However as the angular dimensions become greater its inefficiency increases as the limit of 180° is approached. Graphical visualisation of images of larger angular dimensions is best achieved via a different projection surface such as the spherical[18] one discussed in the following section or by an animated sequence of pictures each with small field of view. The latter would in effect correspond to the observer turning his head and shifting with it his line of sight. However this requires substantially greater computer power. See [9] and [4].

Figure 11 shows the disk with an alternating pattern of white and dark tiles painted on the surface. The colours are chosen so that a tile which is dark on upper side is white on the lower side and vice versa. Note that it is possible to distinguish one side of the disk from the other using the direction of rotation as orientation. Which one calls the 'top' and which the 'bottom' is of course arbitrary. Here the convention will be adopted that the side which appears to be rotating anticlockwise from the point of view of an observer on the axis will be called the 'upper side'. (This is the side of the disk facing the positive ζ axis in the Weyl-Papapetrou-coordinates introduced in chapter 1). This choice of pattern facilitates distinguishing the top from the bottom in images of highly relativistic disks,

[18] One should bear in mind that the human eye is also not a plane surface but a curved one.

where the distortion of the image would otherwise make this much more difficult. Using such a pattern conveys extra visual information about the internal distortion of the picture due partly to the frame dragging effect and partly to the finite speed of light. Also the exact choice of this pattern enables one to separate these general and special relativistic effects (see below). Note that in contrast to changing the opaqueness or the reflectivity of the disk this does probe the effects of the gravitational field via the frame dragging. Figure 12 and the subsequent figures present numerical calculations (see section 2.1.1) of the visual appearance of rigidly rotating dust disks as seen by observers located at the positions indicated.

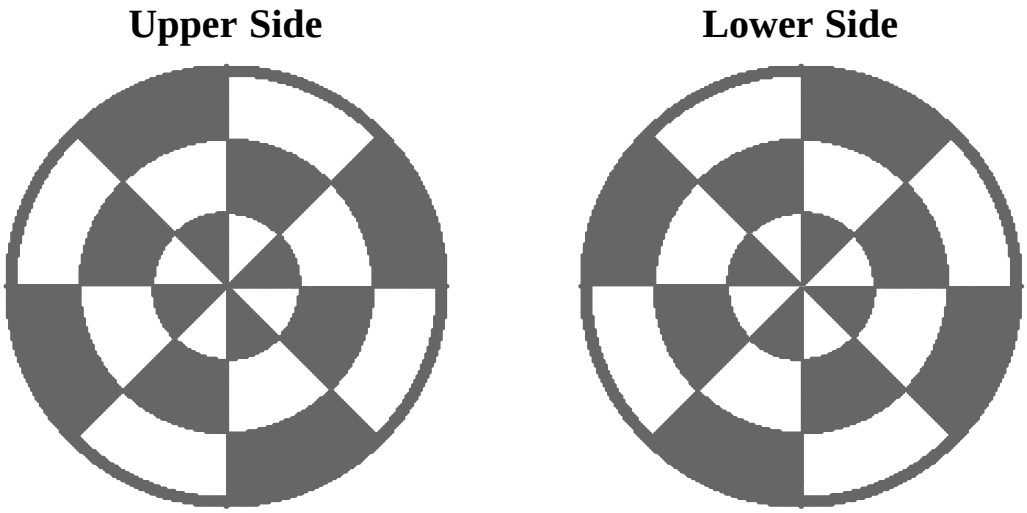

Figure 11: A disk with an alternating 'chessboard' pattern of dark and white tiles.

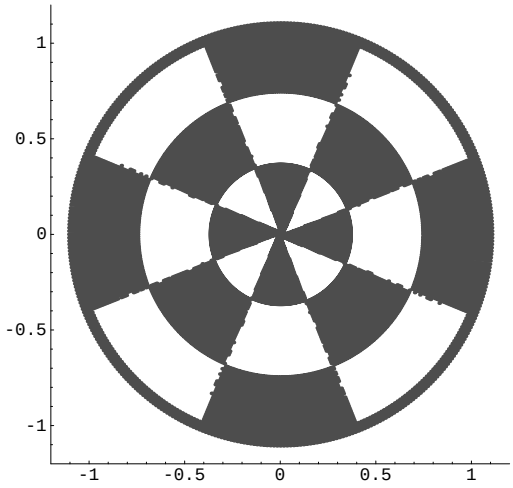

Figure 12: A rotating disk with $\mu = 0.3$ as seen by an observer on the symmetry axis at $\zeta/\rho_0 = 3$. Here as in all other pictures where not explicitly given, the units on the axes are in disk radii.

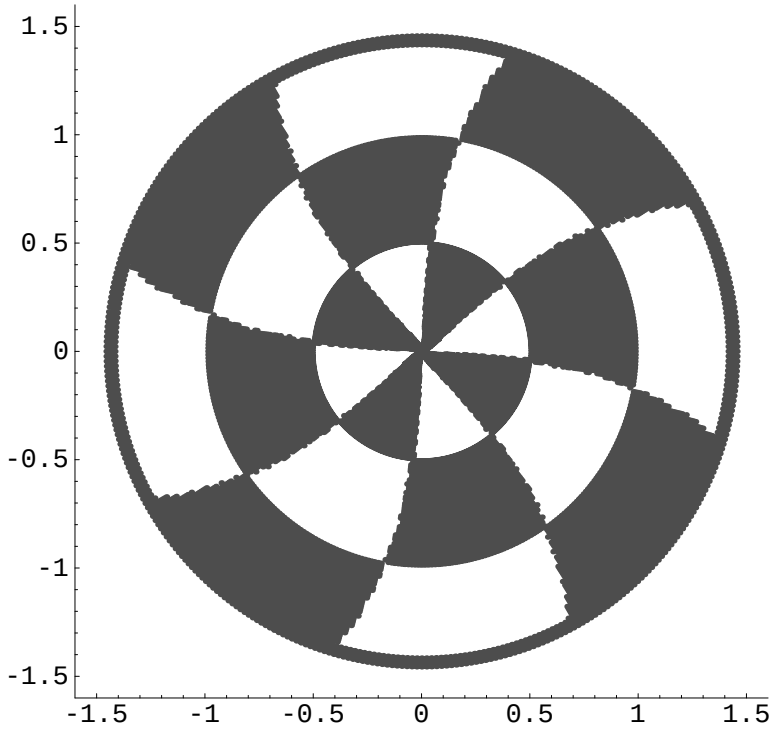

Figure 13: A rotating disk with an $\mu = 1$ as seen by an observer on the symmetry axis at $\zeta/\rho_0 = 3$.

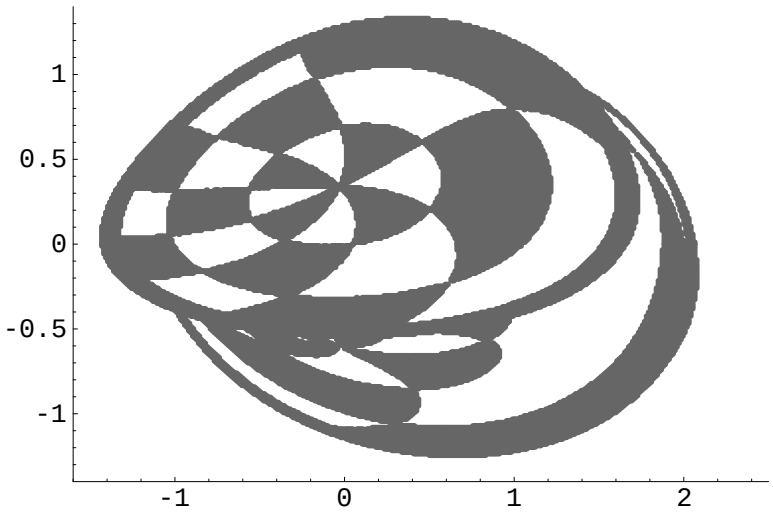

Figure 14: The disk with $\mu = 1$ as seen by an observer located at $\rho/\rho_0 = 5$, $\zeta/\rho_0 = 2$.

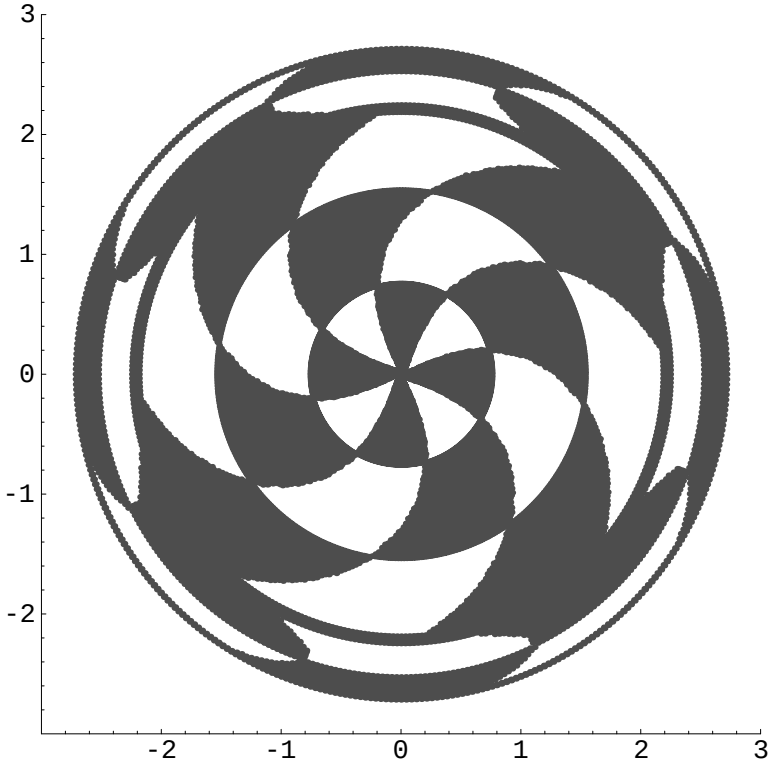

Figure 15: Disk with $\mu = 2$ as seen by an observer on the symmetry axis at $\zeta/\rho_0 = 3$.

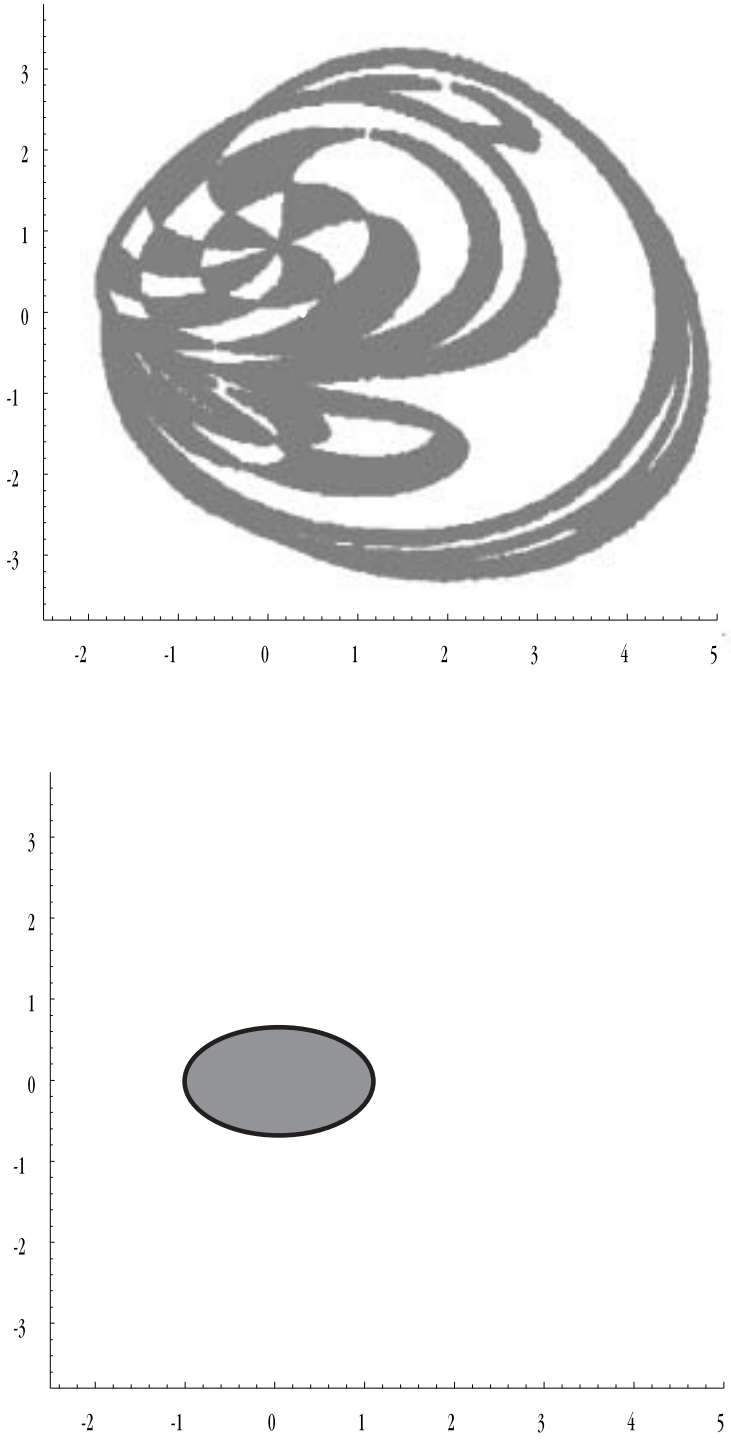

Figure 16: The disk with $\mu = 2$ as seen by an observer located at $\rho/\rho_0 = 10$, $\zeta/\rho_0 = 5$ (upper picture), and the disk as it would look from the same position but without the effects of relativity (lower picture...the chess pattern on the surface has been omitted).

3.2.1 Redshift

The frequency of a light ray as measured by an observer with four velocity u^i at the point of measurement can be given by the formula

$$\omega = -k_i u^i = g_{ij} k^j u^i \tag{25}$$

where k^j can be related to the four momentum p^i of the photon by $k^i = p^i/\hbar$, $\hbar$ being Planck's constant. The four momentum can be related to the conserved quantities L and E introduced in the previous chapter via

$$L = p_i \eta^i \tag{26}$$

$$E = -p_i \xi^i \tag{27}$$

From equation 9 the four velocity u_c^i of a corotating observer located on the surface of the disk (i.e. an observer located at and moving with the particle on the disk emitting the light ray) is

$$u_c^i = e^{-V_o}(\xi^i + \Omega \eta^i) \tag{28}$$

A distant observer at rest has a velocity four vector u_o^i which is proportional to the timelike Killing vector ξ^i

$$u_o^i = \kappa \xi^i \quad (\kappa = const)$$

Also since the worldlines of any real observer must be timelike it follows that

$$u_o^i u_{oi} = u_o^i u_o^i g_{ii} = -1$$

Thus

$$\kappa^2 \xi^i \xi^i g_{ii} = -1$$

Using the fact that in Weyl-Lewis-Papapetrou coordinates $\xi^i = (0, 0, 0, 1)$ and $g_{44} = -e^{2U}$, one then gets[19]

$$\kappa = \frac{1}{\sqrt{-g_{44}}} = e^{-U}$$

[19] any observer at rest would also need to be outside the ergoregion since inside it $g_{44} > 0$ and all bodies are forced to rotate with the disk.

It then follows that

$$u_o^i = e^{-U}\xi^i \tag{29}$$

Combining the equations 28 and 29 with the equation 25 above one arrives at the following relations:

$$\hbar\omega_o = -p_{io}u_o^i = -p_{io}\xi^i e^{-U} = e^{-U}E \tag{30}$$

$$\hbar\omega_c = -p_{io}u_c^i = -p_{io}e^{-V_o}(\xi^i + \Omega\eta^i) = e^{-V_o}(E - \Omega L) \tag{31}$$

where ω_o and ω_c are the photon frequencies as measured by a distant observer at rest and by a corotating observer at the point of emission respectively. Thus the redshift of a photon emitted by the disk with frequency ω_c can be related to the frequency measured by a distant observer at rest by the following equation:

$$\frac{\omega_c}{\omega_o} = e^{U-V_o}(1 - \Omega L/E) \tag{32}$$

This redshift can be calculated and incorporated into pictures as a colouration of the points comprising the images as in figure 17. As described in section 2.1.2, photons which cross the axis of symmetry of the disk have L=0. Thus observers located on the axis see the disk as uniformly redshifted.

In general the distribution of ω_o/ω_c will be similar to that shown in figure 17, the main difference being the maximum and minimum values of ω_o/ω_c. An interesting feature of such redshift calculations is the effect of the rotation. In the absence of rotation one would expect all photons to lose energy in climbing out of the gravitational potential well of the disk. However the rotation of the disk causes those photons emitted with spatial velocities having a positive Euclidean dot product with the spatial velocity of disk (particle) at the point of emission, to actually be blueshifted. Intuitively, the photons seem to be 'slung' away from the left[20] side of the disk with an energy boost more than

[20]the 'left' side with respect to an observer who considers the increasing positive ζ axis to be 'up'.

big enough to offset the energy lost in climbing out of the gravitational potential well. The apparent brightness of the disk as seen by an observer, which is proportional to the energy flux into the observers eye, can also be estimated from this picture. This energy flux is proportional to the measured frequency times the solid angle subtended. Thus $(\vartheta_o\omega_o)/(\vartheta_c\omega_c)$ where ϑ_c and ϑ_o are the solid angles subtended by an area element on the disk and its image respectively, is a measure of the perceived brightness of the area element in question.

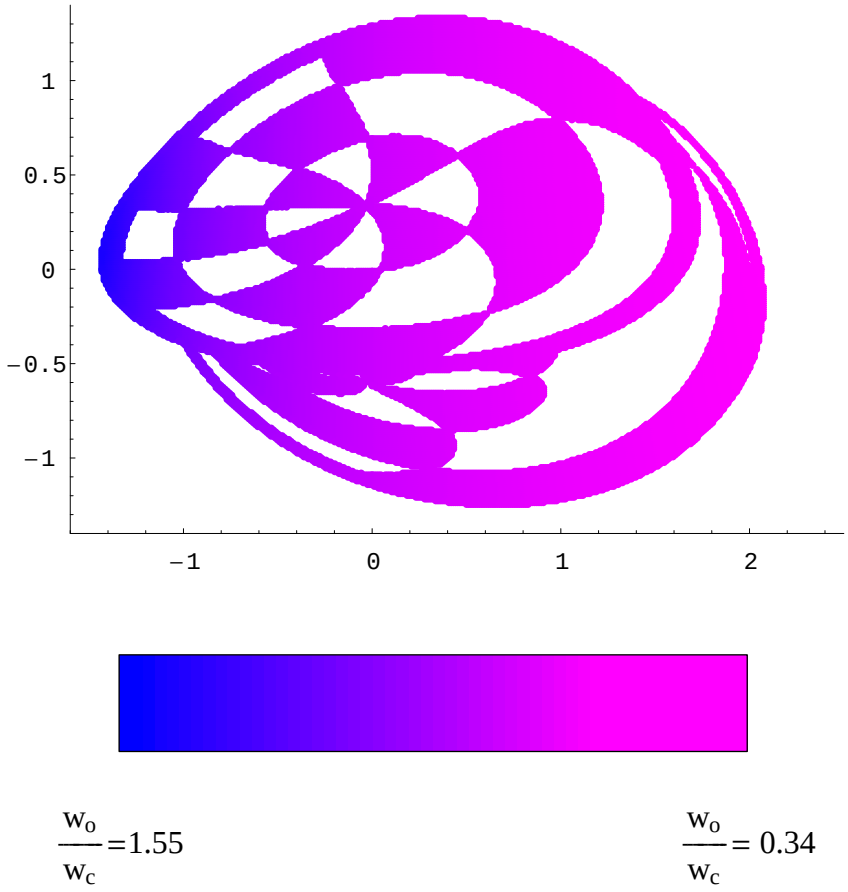

Figure 17: The visual appearance of a relativistically rotating disk which emits (or reflects) light of frequency ω_c. The light reaches an observer located at $\rho/\rho_0 = 5, \zeta/\rho_0 = 2$ with frequency ω_o. Light from the right side is redshifted, while that from the left is blueshifted, with ω_o/ω_c varying between 1.55 and 0.34 as indicated. The rotation of the disk thus overcompensates for the energy the photons on the left side (moving towards the observer) lose in climbing out of the gravitational field, resulting in a net increase of energy. (Intuitively the photons are 'catapulted' at the observer). This image is an interesting illustration of the effects of a rotating gravitational field, since in the absence of rotation all photons would be redshifted.

3.2.2 Special Relativistic Image Distortion

Even in the absence of a gravitational field it is possible for the image to be distorted if both observer and the observed object are moving relatively with a speed with is non-negligible compared to the speed of light.[21] In general the flight time of photons reaching the observer's eye is dependent on the point of emission. The (instantaneous) image perceived by an observer is comprised of photons reaching his/her eye simultaneously, and such photons must then perforce have been emitted at different times. If the object is moving relative to the observer at high speed then the photons (which are not emitted simultaneously) get emitted when the object is at a different position. In the images shown below, the observer position is fixed with respect to the centre of the disk, and the only relative movement is the rotation of the disk.

Consider the rotating disk illustrated in figure 18. Here the finite speed of light can be seen to cause straight lines to look curved and corresponding curved lines to look straight. This fact can be exploited to 'subtract' this special relativistic distortion[22] from images. Instead of allowing photon emission from a corotating 'chessboard' pattern of tiles as has been the case up until now, one could use an imaginary massless 'filter' with a similar pattern encasing the disk but not rotating with it. The effect of such a filter would be to force the light rays to convey an image that is effectively freed from the special relativistic image distortion. Thus a rapidly rotating disk encased in such a filter would appear to an observer as a disk with the same surface pattern but corotating were the speed of light infinite. Images calculated in this way evidence only the effects of general relativity and can be compared to those calculated using a corotating pattern to give one an impression of how much image distortion is a result of the finite speed of light and how much can be attributed directly to the non-rectilinear light rays of general relativity. Note that the outline of the disk should appear the same in both cases since the centre of the disk and its

[21] See eg. [7], [8].

[22] by 'special relativistic' distortion is meant the apparent curvature of straight lines due solely to the finite speed of light which is a direct consequence of Einstein's special theory of relativity.

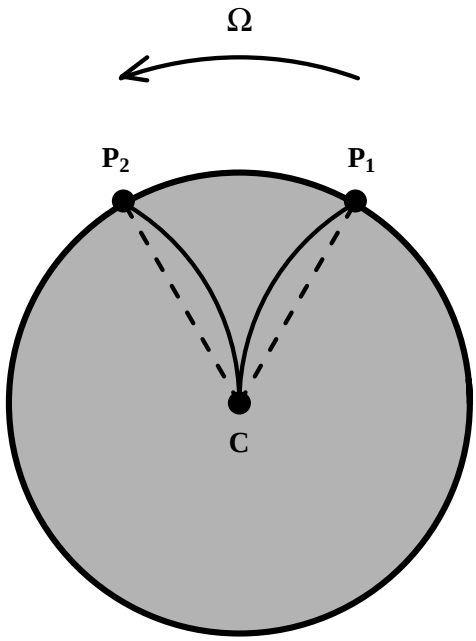

Figure 18: The view of an (for simplicity, axially located) observer of a disk during fast disk rotation of angular speed Ω about the axis of symmetry. The straight line CP_1 appears curved, since the photons emitted from along this line must be emitted when the points in question cross the curved line CP_1 in order to reach the observer's eye simultaneously and thus contribute to the (instantaneous) image of the line. Conversely, if disk particles along the curved line CP_2 emit a photon while crossing the straight line CP_2 these will arrive simultaneously at the observer's eye and thus the curve will appear straight.

axis of rotation remain fixed with respect to the observer and thus only the gravitational field distorts the image's outline through its ray bending influence. (The only relative movement of disk and observer is due to the rotation of the disk; the outline of the disk is fixed as seen by the observer). Figures 19-21 are examples of such images.

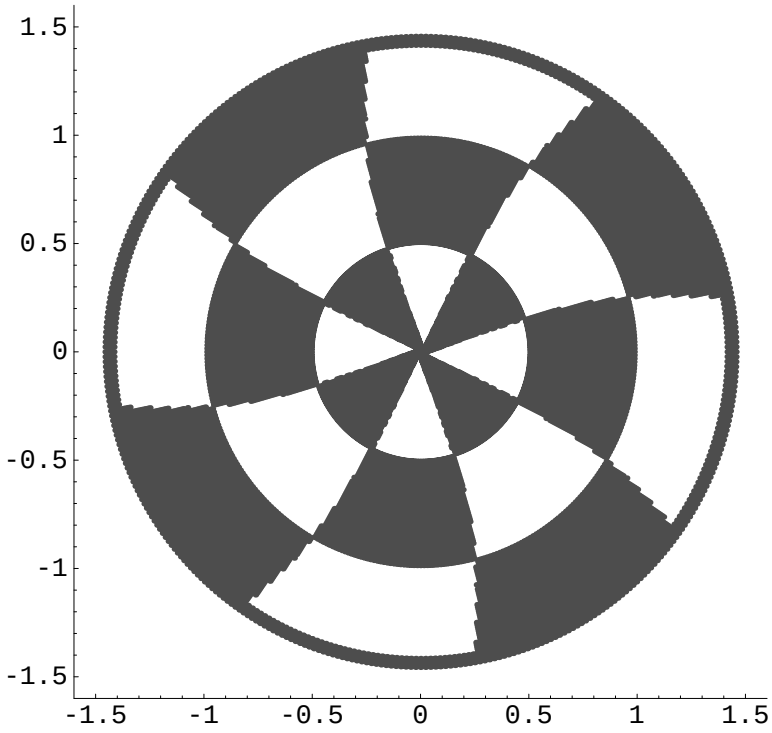

Figure 19: Disk with only general relativistic image distortion included for $\mu = 1$, as seen by an observer on the axis at $\zeta/\rho_0 = 3$. This image should be compared to figure 13.

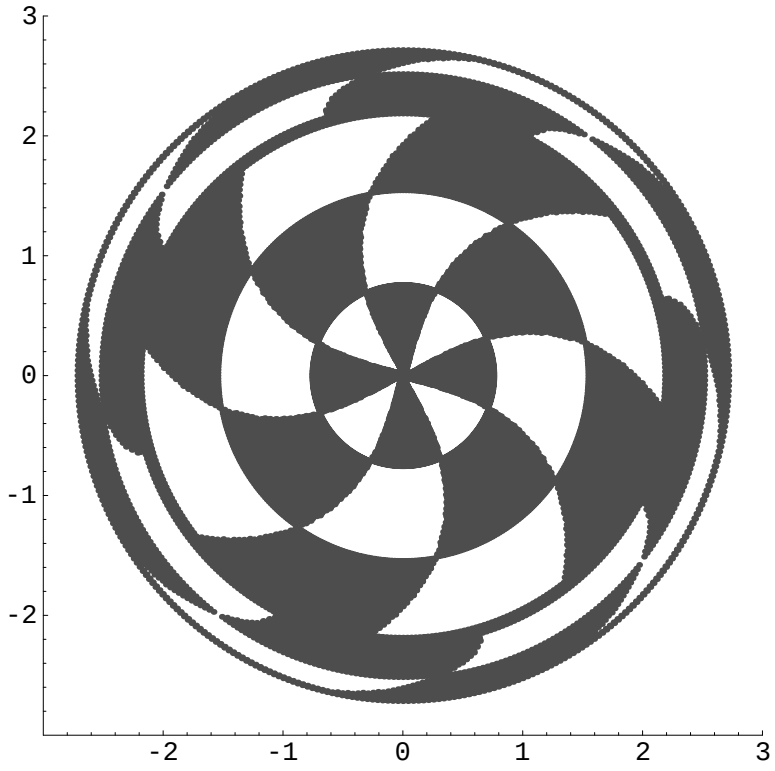

Figure 20: Disk with only general relativistic image distortion included for $\mu = 2$, as seen by an observer on the axis at $\zeta/\rho_0 = 3$. This image should be compared to figure 15.

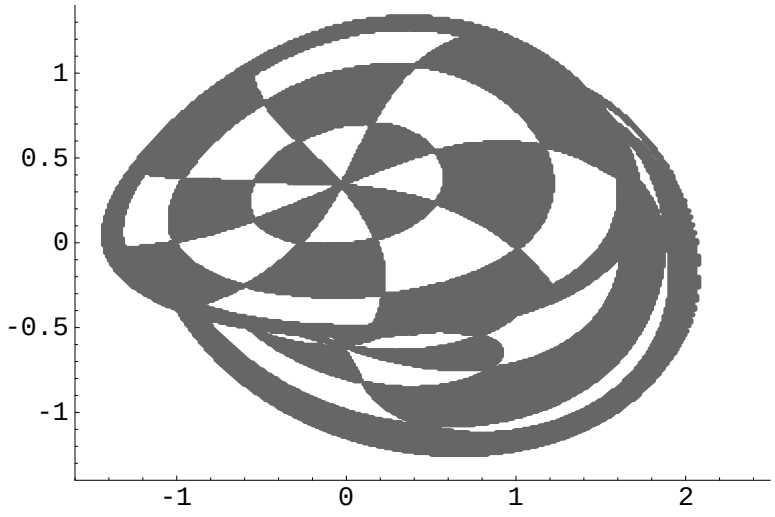

Figure 21: Disk with only general relativistic image distortion included for $\mu = 1$, as seen by an observer located at $\rho/\rho_0 = 5$, $\zeta/\rho_0 = 2$. This image should be compared to figure 14.

3.3 Spherical Projection Surface

Figure 22 shows the disk image projected onto a spherical projection surface of radius equal to the distance of observer to the centre of the disk. (The radius of the sphere is not of great consequence. However, choosing the radius so that the disk lies tangentially to it makes it easier to see the apparent size of the disk[23]). The observer is always located at the centre of the sphere and so it can in a real sense be considered to be the 'sky' of the observer. This is similar to our view of the heavens. The night sky is in essence a spherical surface onto which the positions and apparent sizes of the celestial bodies are projected. One should bear in mind that although one can choose from many projection surfaces there is just one image which they represent. What an observer sees is completely independent of the methods used here to convey this view, as it should be. The eye understands just one coordinate system.[24]

On increasing the value of the relativistic parameter one witnesses the appearance of 'second order' images (see figure 24). These secondary images are a result of light rays which pass through the plane of the disk outside the rim but do not continue on to reach spatial infinity (see figure 23). Instead they reverse their direction and return to hit the disk from the other side.

As the value of μ is increased further even higher order images appear corresponding to rays that circle the disk many times before finally being captured. In general such rays follow very complicated paths that are difficult to describe as 'regular' in the naive sense of the word, as can be illustrated in figure 25.

[23]provided the observer knows how far from the disk he is he can judge its apparent size from the solid angle it subtends. This also applies to the flat projection surface

[24]To further complicate matters one could consider that although the surface in e.g. figure 22 is called 'spherical' it is in fact more precisely the projection of a spherical surface onto a flat page! The reader's imagination is called upon to interpret these pictures as they are intended, namely three dimensional. Thankfully Einstein's theory describes the world in terms of 'only' four dimensions, despite the diligent efforts of many theoretical physicists to increase this number...the success of which efforts would make visualisation, already difficult enough, a truly formidable task!

Closer examination of the higher order images as in figure 27 reveals a pattern which is much more regular than the paths of the light rays giving rise to them. In fact, detailed studies of this pattern by Weiskopf and Ansorg [9] on the Cray T3E/512 supercomputer in Stuttgart indicate that this pattern is self-similar up to at least 5 orders of magnification. Here is meant that magnification of a small section of the (upper part of the) pattern shown in figure 27 reveals a pattern which is indistinguishable from the original bigger section from which it was cut. Furthermore, that repeatedly cutting out a small section and again magnifying it produces the same result. This remarkable fact seems to strongly suggest that there may be a fractal geometry hidden in the higher order images. It would indeed be remarkable if chaos and fractal geometry emerged in general relativity through the wild 'spaghetti' rays of figure 25 and the self repeating patterns of figure 27. A strict mathematical proof irrefutable by the most cautious of scientists that this is the case is unfortunately not afforded by such numerical studies, but perhaps spurred on by the tantalising possibility such a proof may be attainable in the not too distant future.

As remarkably demonstrated by figure 27 the observer could look in the opposite direction and still see the disk. Also noteworthy is that in none of the pictures calculated did disjoint images appear. This means that the image of the disk as presents itself to an observer is always (or to be more precise anything else has never been calculated) composed of a single object with no holes (topologically compact and simply connected). This is in contrast to the case where the disk is no longer the source of light but only of the gravitational field. This is the topic of chapter 4 where lensing is discussed. Here light rays emanating from a body are influenced by the disk (located roughly between observer and the light source being imaged), in such a fashion that the resulting image can in fact be composed of many spatially (and in general temporally) separated objects. One speaks in this case of the *images* of such a body.

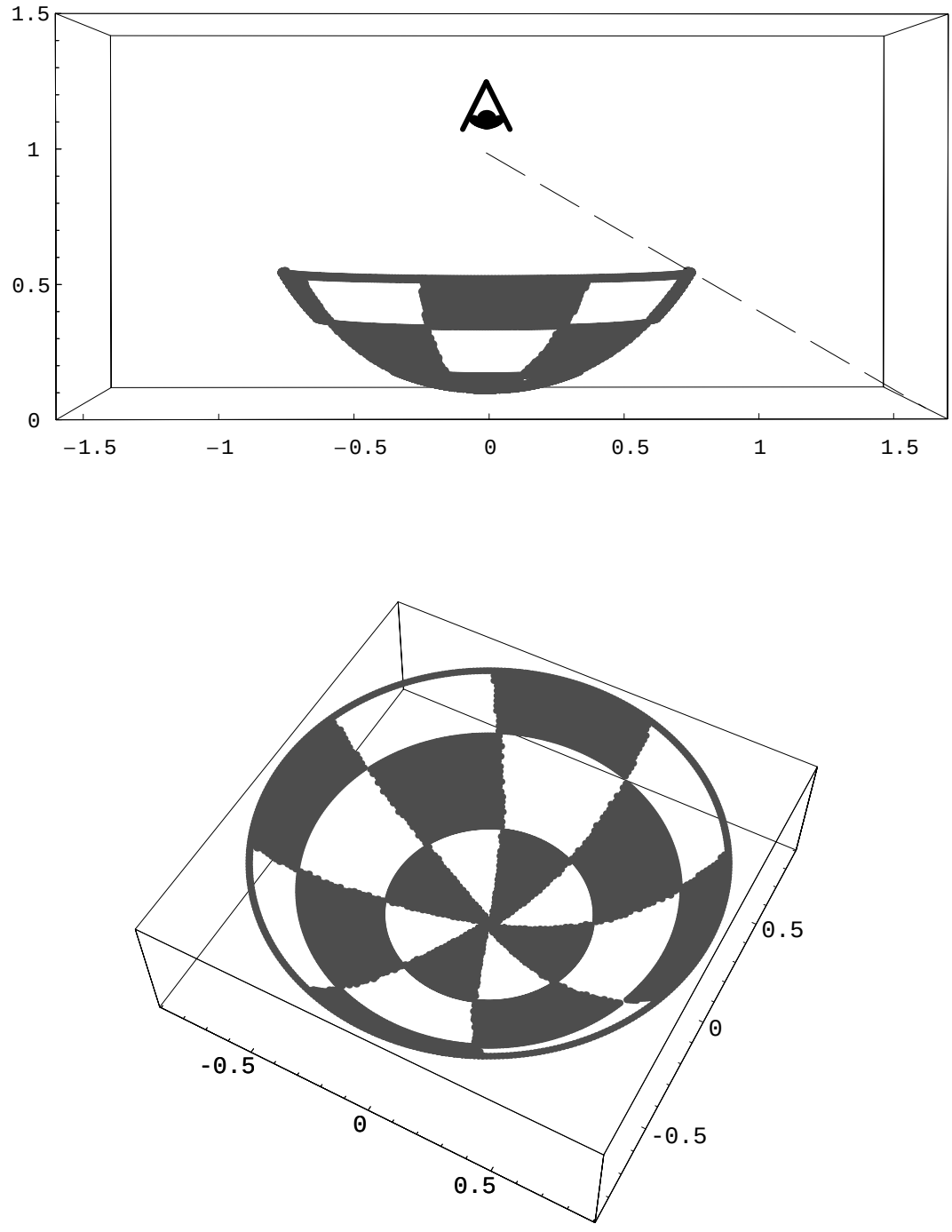

Figure 22: The disk with $\mu = 1$, $\zeta/\rho_o = 1$ represented on a spherical projection surface. The equivalent representation on a flat projection surface is alluded to by the dotted line in the upper picture.

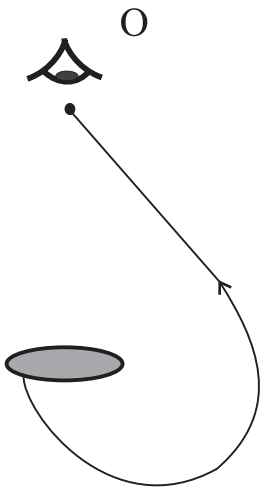

Figure 23: A typical light ray which gives rise to second order images as seen by an observer labelled O.

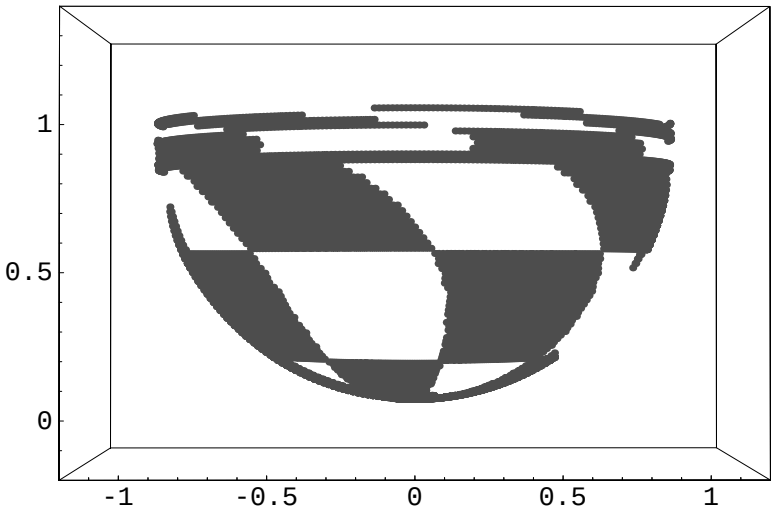

Figure 24: The disk with $\mu = 2.5$, $\zeta/\rho_o = 1$ represented on a spherical projection surface. The upper part of the image (near the 'equator' of the sphere) is the result of second order light rays.

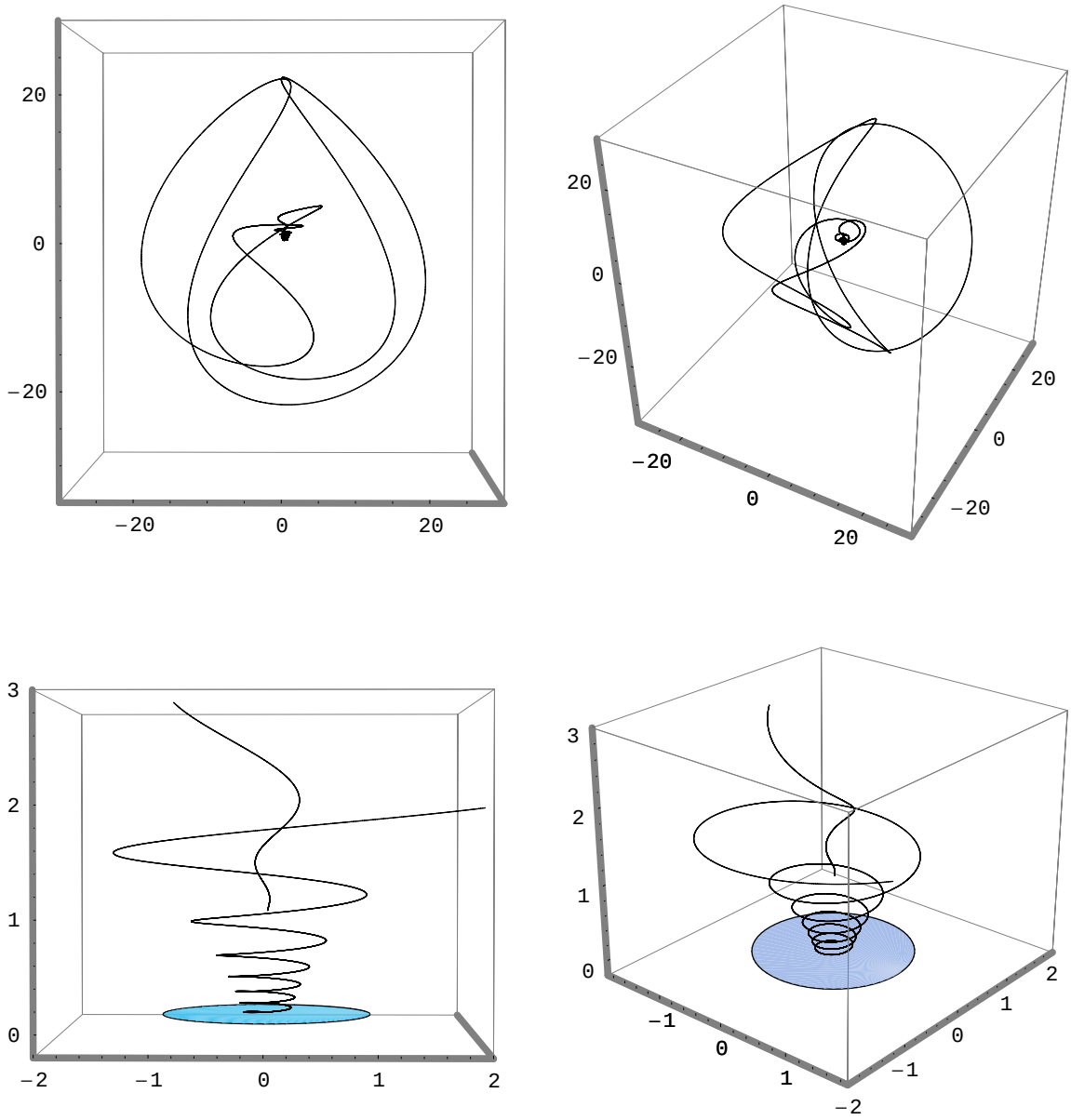

Figure 25: A light ray calculated for $\mu = 4.4$, $\zeta/\rho_o = 1$ which, after crossing the disk plane six times, finally strikes the disk. Left and right show the same scene but from a different angle of view. The lower pair of pictures are magnifications of the central portions of the upper ones.

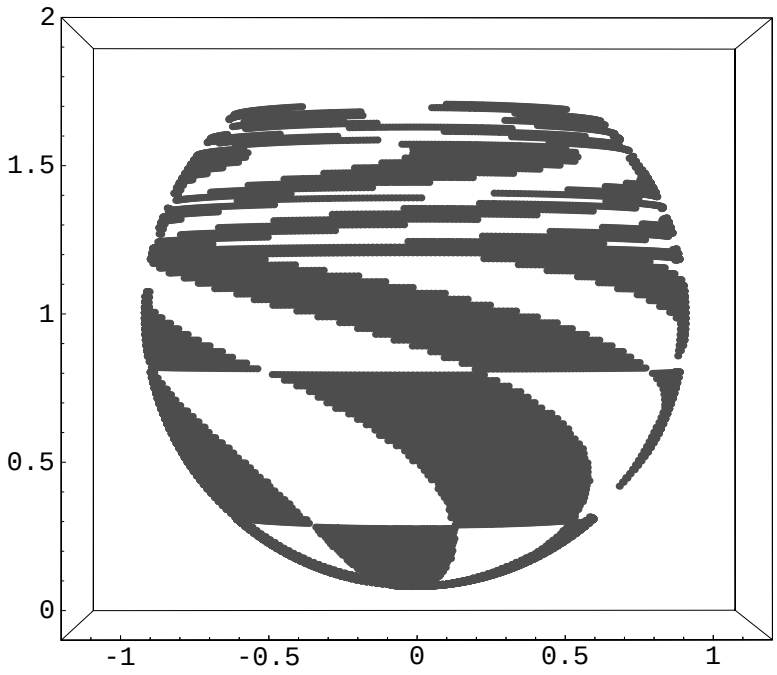

Figure 26: $\mu = 3.5$, $\zeta/\rho_o = 3$.

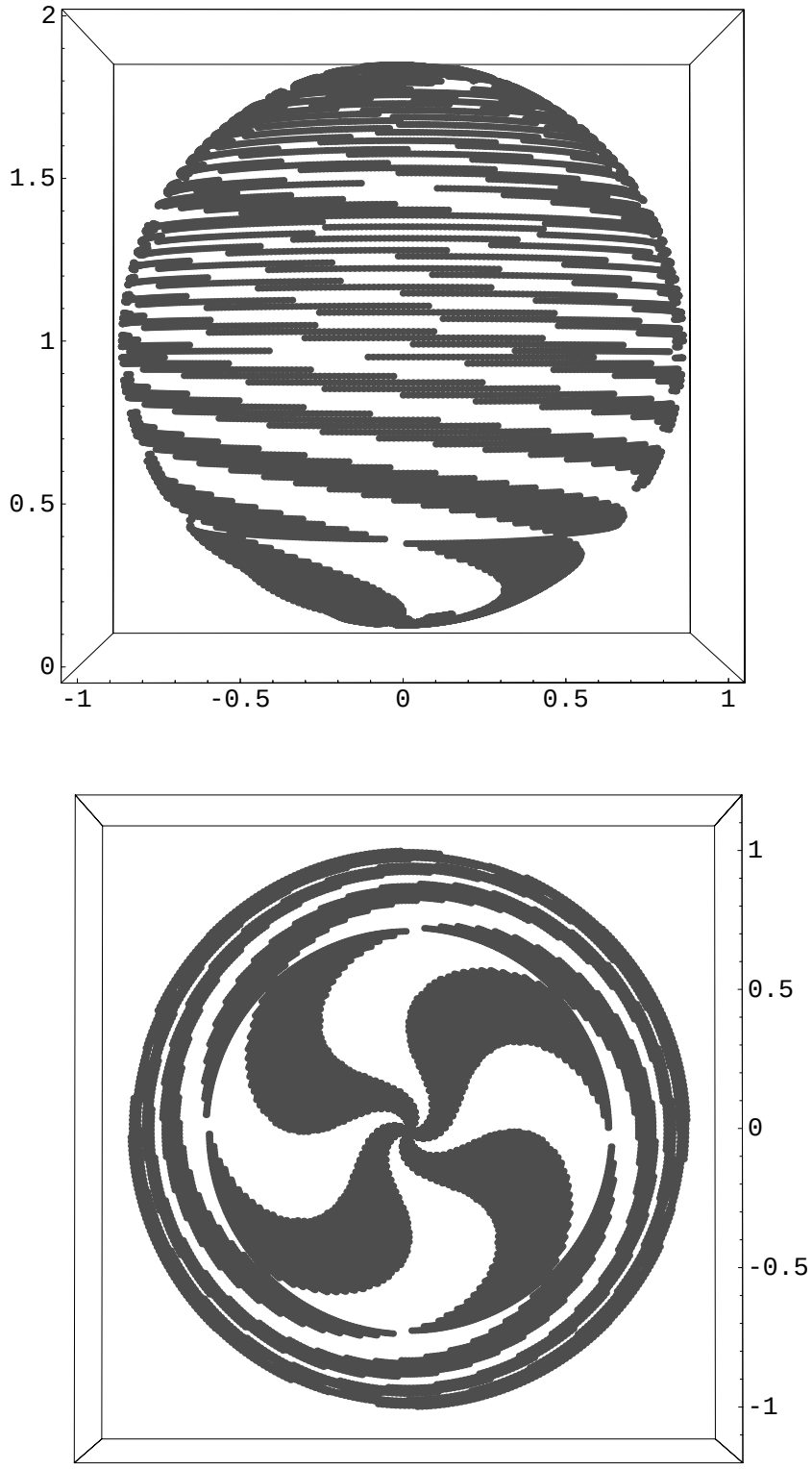

Figure 27: Disk with $\mu = 4.4$ (extremely relativistic), $\zeta/\rho_o = 1$. The lower of the two pictures is the underside ($\zeta < 0$) of the spherical projection surface.

4 The Deflection of Light Rays by Rotating Disks

One of the first experimental tests of Einstein's theory of general relativity was the measurement by Eddington of the deflection of a light ray by the sun during a solar eclipse in 1919. General relativity predicts[25] a deflection angle which is given by

$$\alpha = \frac{4GM}{rc^2} \tag{33}$$

Here G is Newton's universal constant of gravitation, M is the mass of the sun, r is the impact parameter, and c is the speed of light. The results of Eddington's observations were in satisfactory agreement with this expression and the name 'Einstein' became engraved in history.[26]

This expression, although concise and very useful, is restricted by the Schwarzschild solution from which it is derived, to the weak exterior gravitational fields of spherically symmetric mass distributions. In the following sections an analytical expression will be derived in the case of a rigidly rotating pressure free ideal fluid disk, and numerical investigation of both rigidly and non-rigidly rotating disks provide an interesting means of comparison of the two.

[25] as can be derived using the Schwarzschild metric describing the gravitational field outside a spherically symmetric massive body under the further assumption that the quantity $M/r << 1$, which is fulfilled in the case of a light ray grazing the sun which is not compact or massive enough to violate this condition

[26] The newspapers of the day featured popular articles about the strange curved four dimensional world in which we live and the imagination of a war torn world was fired by the thought, not to mention the fact that the expedition to the North Pole was lead by an English scientist attempting to confirm the theory of a German one.

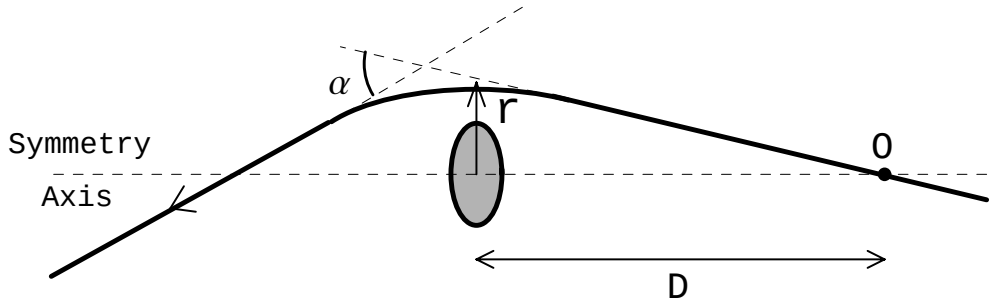

Figure 28: A light ray passes through the symmetry axis of the disk at the point O, which is located a distance D from the centre of the disk. The ray, under the influence of the gravitational field of the rotating disk undergoes a deflection α, which is defined here as the angle between the tangent to the ray at O and the tangent to the asymptotic outgoing ray. In this diagram, the ingoing ray is to be interpreted as in the plane of the page but the light ray does not in general remain so because of the dragging effect of the field due to the rotation of the disk. Note that on account of the reversibility of light rays the photon could equally be considered to be asymptotically ingoing in the opposite direction. The 'impact vector' r, is confined to the disk plane.

4.1 Analytical Approximation for Rigidly Rotating Disks

4.1.1 The Kopeikin-Schäfer Lorentz Covariant Theory of Light Propagation

In 1999 Kopeikin and Schäfer [10] constructed a Lorentz covariant theory of the propagation of light in the (weak) gravitational fields of N-body systems consisting of arbitrarily moving point-like bodies with constant masses m_a (a=1,2,...,N). In this post-Minkowskian treatment the gravitational field is presented in the form of $Liénard-Wiechert$ potentials and depends on coordinates, x_a (a=1,2,...N), and the velocities, $\boldsymbol{v}_a$ of the bodies taken at retarded instants of time. The relativistic equations of light propagation are integrated in the field of the $Liénard-Wiechert$ potentials and there is no restriction on the motion of the bodies except $|\boldsymbol{v}_a| < c$ (speed of light).

Among the many results in this extensive treatise they give an explicit expression for

the deflection of a light ray by this gravitational field. By imposing restrictions on the mass distribution and some further (astrophysically very acceptable) assumptions, their expression can be used to derive an analytical approximation for the deflection suffered by a light ray in the gravitational field of a rigidly rotating disk of dust.

In the Kopeikin-Schäfer theory the metric is prescribed as that of the Minkowski spacetime $\eta_{\alpha\beta} = diag(-1, +1, +1, +1)$, plus a perturbation, $h_{\alpha\beta}$, which is linear in the Newtonian gravitational constant, G.

$$g_{\alpha\beta}(t, \boldsymbol{x}) = \eta_{\alpha\beta} + h_{\alpha\beta}(t, \boldsymbol{x}) \tag{34}$$

Here t is the coordinate time and $\boldsymbol{x} = x^a = (x^1, x^2, x^3)$ are spatial coordinates.[27] By using the Einstein field equations one arrives (see e.g. [16]) at the following equation for $h_{\alpha\beta}$

$$\Box h_{\alpha\beta}(t, \boldsymbol{x}) = -16\pi G S_{\alpha\beta}(t, \boldsymbol{x}) \tag{35}$$

where

$$S_{\alpha\beta}(t, \boldsymbol{x}) = T_{\alpha\beta}(t, \boldsymbol{x}) - \frac{1}{2}\eta_{\alpha\beta} T^{\lambda}_{\lambda}(t, \boldsymbol{x}) \tag{36}$$

and $\Box$ is the d'Alembert operator: $\Box = \eta^{\alpha\beta}\partial_\alpha\partial_\beta$. The energy-momentum tensor $T^{\alpha\beta}$, as given in covariant form in [17], is

$$T^{\alpha\beta}(t, \boldsymbol{x}) = \sum_{a=1}^{N} \hat{T}^{\alpha\beta}(t)\delta(\boldsymbol{x} - \boldsymbol{x_a}(t)) \tag{37}$$

with

$$\hat{T}^{\alpha\beta}(t) = m_a \gamma^{-1}(t) u^{\alpha}_a(t)) u^{\beta}_a(t) \tag{38}$$

Here m_a is the (constant relativistic) mass of the a-th particle in the light deflecting mass distribution. The (time dependent) Lorentz factor $\gamma_a(t) = (1 - v^2_a(t))^{-1/2}$, $u^{\alpha}_a(t)\gamma_a(t), \gamma_a(t)\boldsymbol{v}_a(t)$ is the four-velocity of the a-th particle and $\delta(\boldsymbol{x})$ is the usual three dimensional Dirac delta function.

[27] Greek indices take values from 0 to 3 and are raised and lowered with the Minkowskian metric $\eta_{\alpha\beta}$, whereas Latin indices range from 1 to 3 and are raised and lowered with the Kronecker delta (i.e. components with upper and lower Latin indices are indistinguishable). All terms with repeated upper and lower indices are taken to be added according to the Einstein summation convention. Unless stated otherwise bold letters represent (spatial) three-vectors.

Equation 35 can then be solved to yield the retarded $Liénard-Wiechert$ potential $h_{\alpha\beta}$

$$h_{\alpha\beta}(t,\boldsymbol{x}) = 4G\sum_{a=1}^{N}\frac{\hat{T}_a^{\alpha\beta}(s) - \frac{1}{2}\eta^{\alpha\beta}\hat{T}^{\lambda}_{\lambda a}}{r_a(s) - \boldsymbol{v}_a(s)\cdot\boldsymbol{r}_a(s)} \tag{39}$$

where the "$\cdot$" symbolises the Euclidean dot product and the retarded time $s = s(t,\boldsymbol{x})$ for the a-th body is a solution of the light-cone equation

$$s + |\boldsymbol{x} - \boldsymbol{x}_a(s)| = t \tag{40}$$

This expression for $h_{\alpha\beta}(t,\boldsymbol{x})$ is Lorentz covariant and valid in any harmonic coordinate system admitting a smooth transition to the asymptotically flat spacetime at infinity, where such systems can be related to each other by the Lorentz transformations of special relativity (see [18]).

The equation for the propagation of a light ray in Minkowski spacetime is

$$x^i = x_0^i + k^i\ \ (t - t_0) \tag{41}$$

Here $\boldsymbol{k} \equiv k^i$ is defined by the equation

$$\boldsymbol{k} = \frac{d\boldsymbol{x}(-\infty)}{dt} \tag{42}$$

with $\boldsymbol{k}^2 = 1$, and $k^\alpha = (1, k^i)$, and its prescription serves as a boundary condition for the photon motion. Furthermore, the stipulation of

$$x_0^i \equiv x^i(t_0) \tag{43}$$

acts as an initial condition. An independent parameter τ along the photon's trajectory may be defined via

$$\tau = \boldsymbol{k}\cdot\boldsymbol{x}(t) \tag{44}$$

Kopeikin and Schäfer derived the equations for the null geodesics which read as follows:

$$\ddot{x}^i(\tau) = \frac{1}{2}k_\alpha k_\beta\hat{\partial}_i h^{\alpha\beta}(\tau,\hat{\boldsymbol{r}}) - \hat{\partial}_\tau\left[k_\alpha h^{\alpha i}(\tau,\hat{\boldsymbol{r}}) + \frac{1}{2}k^i h^{00}(\tau,\hat{\boldsymbol{r}}) - \frac{1}{2}k^i k_p k_q h^{pq}(\tau,\hat{\boldsymbol{r}})\right] \tag{45}$$

where the constant vector $\hat{r}^i \equiv \hat{\boldsymbol{r}} = \boldsymbol{k}\times(\boldsymbol{x}_0\times\boldsymbol{k})$, with the symbol '$\times$' denoting the Euclidean cross product of two vectors. The impact parameter $\hat{\boldsymbol{r}}$, of the unperturbed light ray is perpendicular to the vector $\boldsymbol{k}$.

By integrating equation 45 and using equation 39, Kopeikin and Schäfer were able to obtain an explicit expression for the deflection angle $\alpha^i(\tau)$, due to an N-body mass distribution in a first post-Minkowskian approximation. After specification of the asymptotic tangent $\boldsymbol{k}$ and the time t_0, (this is equivalent to specifying the distance D in figure 28) one can calculate the resulting deflection from the formula:

$$\alpha^i(\tau) = 2G\sum_{a=1}^{N}\frac{m_a}{\sqrt{1-v_a^2}}\frac{(1-\boldsymbol{k}\cdot\boldsymbol{v}_a)^2}{q_a-\boldsymbol{k}\cdot\boldsymbol{q}_a}\frac{P_j^i r_a^j}{q_a-\boldsymbol{v}_a\cdot\boldsymbol{q}_a} - 4G\sum_{a=1}^{N}\frac{m_a}{\sqrt{1-v_a^2}}\frac{1-\boldsymbol{k}\cdot\boldsymbol{v}_a}{q_a-\boldsymbol{v}_a\cdot\boldsymbol{q}_a}P_j^i v_a^j \tag{46}$$

Here P_{ij} is a projection operator which projects vectors onto the plane orthogonal to the vector $\boldsymbol{k}$ and is given by the expression $\delta_{ij} - k_i k_j$. Furthermore, $\boldsymbol{q_a} \equiv \boldsymbol{x} - \boldsymbol{x}_a$ and $q_a \equiv x - x_a$. All quantities in equation 46 describing the a-th body of the light deflecting mass distribution have to be taken at the retarded time s. (In the application of the equation to a rotating disk however, this consideration of the retarded time will become unimportant due to the stationarity of the disk configuration). Treating an angle as a vector in such a way as to decompose it into 2 components is an operation only valid for small angles (just as a small element of the surface of a 2-sphere can be well approximated by its projection onto the tangent plane provided the surface element in question is small). This assumption is valid in this post-Minkowskian approximation as the resulting angles are indeed acceptably small. (See equations 51 and 52 for a quantitative expression).

4.1.2 The Deflection Angle

If one considers the configuration of the light deflecting mass distribution to be that of a rigidly rotating disk the summations in equation 46 become integrals since the N-bodies of the Kopeikin-Schäfer theory become a continuous mass distribution. The approximation will be made that the mass density profile $\sigma(\rho)$ of the disk be that of a Newtonian disk[28]

[28]This is not a significant sacrifice of generality since the formula 46 already supposes a linear dependence on the Newtonian gravitational constant. Also referring to figure 2 one can see that the surface

$$\sigma(\rho) = \frac{2\Omega^2}{\pi^2 G}\sqrt{\rho_0^2 - \rho^2} \tag{47}$$

Additionally the conditions $v_a << c$ (by only considering terms of at most order v_a/c) and $r << D$ will be imposed, both of which are astrophysically very plausible. (Among other complications, inclusion of terms of higher order would be inconsistent with the use of equation 47 for the surface mass density. See [19] and [20] for details). One can use equation 46 to arrive at the following expression[29] for the deflection angle suffered by the light ray depicted in figure 28.

$$\boldsymbol{\alpha}(\boldsymbol{r}) = \frac{4G}{c^2}\int_{\rho'=0}^{\rho_0}\int_{\phi'=0}^{2\pi} \sigma\,(1 - \boldsymbol{\kappa}\cdot\boldsymbol{v}/c)\frac{1 - \boldsymbol{\kappa}\cdot\boldsymbol{v}/c}{\sqrt{1 - \boldsymbol{v}^2/c^2}}\,\frac{\boldsymbol{r} - \boldsymbol{\rho'}}{|\boldsymbol{r} - \boldsymbol{\rho'}|^2}\,\rho' d\phi' d\rho' \tag{48}$$

Here $\boldsymbol{\rho'}$ is the position vector of mass elements on the disk with respect to the centre of the disk, $\boldsymbol{\rho'} = \rho'(\cos\phi', \sin\phi')$, and $\boldsymbol{r} = r(\cos\phi, \sin\phi)$ is the impact vector.[30] The 3-vectors $\boldsymbol{\kappa}$ and $\boldsymbol{v}$ are given by

$$\boldsymbol{\kappa} = \left(\frac{\boldsymbol{\rho'}}{D}, 1\right) \tag{49}$$

$$\boldsymbol{v} = \boldsymbol{\Omega} \times \boldsymbol{\rho'} \tag{50}$$

with the angular velocity $\boldsymbol{\Omega}$, being a 3-vector of magnitude Ω which points in the direction orthogonal to the plane of the disk. Equation 48 can be integrated to yield the following expressions for the radial (angle between the projections of the ingoing and outgoing rays onto the plane containing the symmetry axis and the impact vector) and

mass density profile is not strongly dependent on the value of the relativistic parameter μ (for moderate values of μ) so that one would expect that in the case where only a linear dependence on the gravitational constant is under consideration (i.e. very small values of μ), that a Newtonian mass density profile would be more than sufficient.

[29] In the remainder of this section the constant c will be included explicitly so as to illustrate the dimensionlessness of the expression for the deflection angle. One should note however, that in the rest of this thesis units are adopted in which c=1

[30] (r, ϕ),(ρ', ϕ') are simply plane polar coordinates in the disk plane, analogous to the ρ and ϕ coordinates of the Weyl-Lewis-Papapetrou-system. One should note that the set of values of the impact parameter r, really trace out the coordinate axis in ρ-space, but the impact parameter is denoted here by 'r' instead of ρ to conform to standard literature, and to differentiate it from the coordinate proper

tangential (...plane containing the symmetry axis and perpendicular to the impact vector) components of the deflection angle.

$$\alpha_r = \frac{16\rho_0^3\Omega^2}{3\pi r c^2} \tag{51}$$

$$\alpha_t = \frac{16\rho_0^5\Omega^3}{15\pi D r c^3} \tag{52}$$

Both radial and tangential components of the deflection angle decrease linearly with the impact parameter r, as is the case for a Schwarzschild deflecting mass in a weak field approximation (see equation 33 above). Interestingly however, only the (much smaller) tangential component depends on the distance D, such that for a light source (corresponding to O in figure 28) located far from the disk the light ray would only be deflected radially. This scenario has ramifications for physical observations, a typical astrophysical setting being for example light from distant star being deflected by a galaxy located between the earth (where the 'outgoing' ray would be measured) and the star. One may note that if one had neglected all terms of order v/c in the integrand above one would have still arrived at the same expression for α_r, but α_t would have been zero. This would have been equivalent to having used

$$\alpha^i(\tau) = 2G\sum_{a=1}^{N}\frac{m_a}{q_a}\frac{P^i_j q^j_a}{(q_a - \boldsymbol{k}\cdot\boldsymbol{q}_a)} \tag{53}$$

instead of equation 46. Also, integrating equation 47 over the disk yields

$$M = \frac{4\rho_0^3\Omega^2}{3\pi G}$$

for the mass of the disk. Combining this expression with equation 51 reproduces equation 33. In this sense α_r is a zeroth order contribution and α_t a first order correction term to the total deflection $\alpha = \sqrt{\alpha_r^2 + \alpha_t^2}$.

The deflections predicted by the formulae 51 and 52 can be checked for agreement with numerical values obtained from the Neugebauer-Meinel solution. (See figure 30 for details).

4.2 Numerical investigation of highly relativistic Rotating Disks

Using the Neugebauer-Meinel and Ansorg-Meinel solutions one can numerically calculate the deflection angle depicted in figure 28 to a high degree of accuracy, even for extremely relativistic gravitational fields, where the resulting deflections are as large as 360°.[31] In fact this investigation proves to be one of the most enlightening means of contrasting the rigidly and non-rigidly rotating disks, since the radial coordinate is the variable as a function of which the two disk classes[32] can be considered to differ ($\Omega = \Omega(\rho)$). One can readily plot the deflection as a function of the impact parameter (itself a radial parameter), for several values of $\Omega\rho_0$, thus gaining intuitive and quantitative insight into the physical expression of this dependence/independence of the angular velocity on the radial coordinate, and how it changes as the gravitational field becomes more relativistic. In order to make a sensible comparison of a rigidly rotating and a differentially rotating disk however, one requires a criterion according to which a differentially rotating disk can be considered 'equivalent' to a rigidly rotating counterpart, in the sense that they can be considered 'equally relativistic' in a well defined and meaningful way. One criterion which lends itself to this purpose is the value of M^2/J (see equations 15,16). One could conceivably generalise the definition (see equation 13) of μ to differentially rotating disks by, for example, replacing Ω by an average weighted by the surface mass density. The quantity M^2/J however, is more suitable and allows a direct comparison as exhibited in figure 9.

The results of these numerical investigations are shown below in figures 31-33. The dotted (dashed) curves correspond to differentially rotating disks with a surface mass density which increases (decreases) as a function of the radial coordinate. The solid lines represent rigidly rotating disks. To further illuminate the physical properties of the disks involved, each of the three graphs shown is accompanied by a plot of $\Omega(\rho)$, the angular

[31] Even more extreme deflections than those of 360° are possible, as figure 25 clearly demonstrates. However the results here will concentrate on deflections in the range of 0-360°.

[32] Visualisation (as in chapter 3) of differentially rotating rotating disks, and calculation (as in chapter 5) of their caustic structure are also possible. Such studies have shown however, that the most illustrative comparison of differentially and rigidly rotating disks is afforded by the deflection angle.

velocities as a function of the radial coordinate.

One can also calculate the maximum (w.r.t. the impact parameter) deflection as a function of the relativistic parameter (μ for the rigidly rotating disk). This maximum deflection corresponds to light rays which just graze the edge of the disk, and for the rigidly rotating disk is plotted in figure 29.

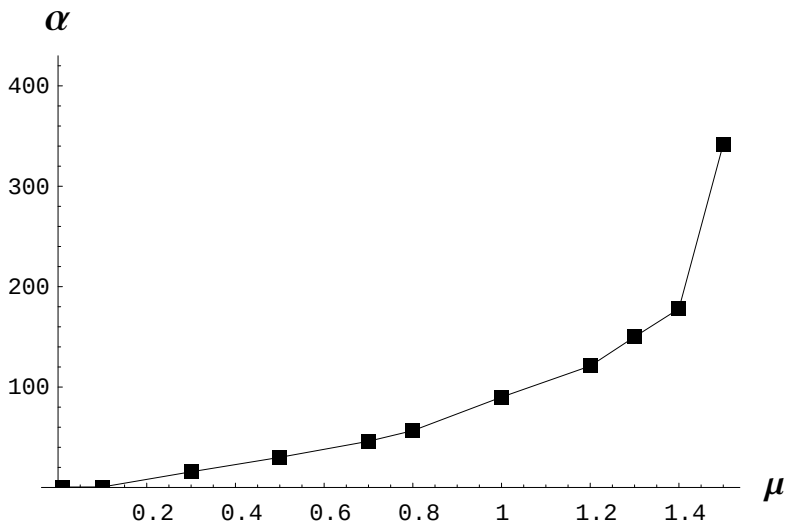

Figure 29: The deflections (in degrees) α, of the 'grazing rays' which pass the disk plane ($\zeta = 0$), negligibly close to the edge of the rigidly rotating disk.

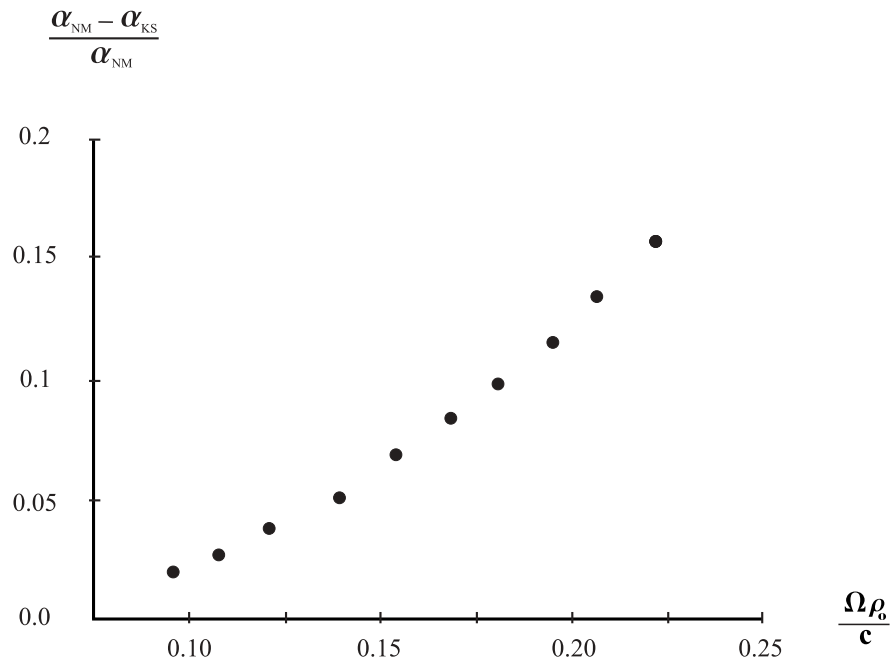

Figure 30: The fractional difference between values for the total deflection angle obtained from the analytical approximation using the Kopeikin-Schäfer theory (equations 51 and 52 with $\alpha_{KS} = \sqrt{\alpha_r^2 + \alpha_t^2}$), and corresponding values obtained by numerically integrating the null geodesics using the Neugebauer-Meinel solution (α_{NM}). The impact parameter in question was slightly greater than ρ_0.

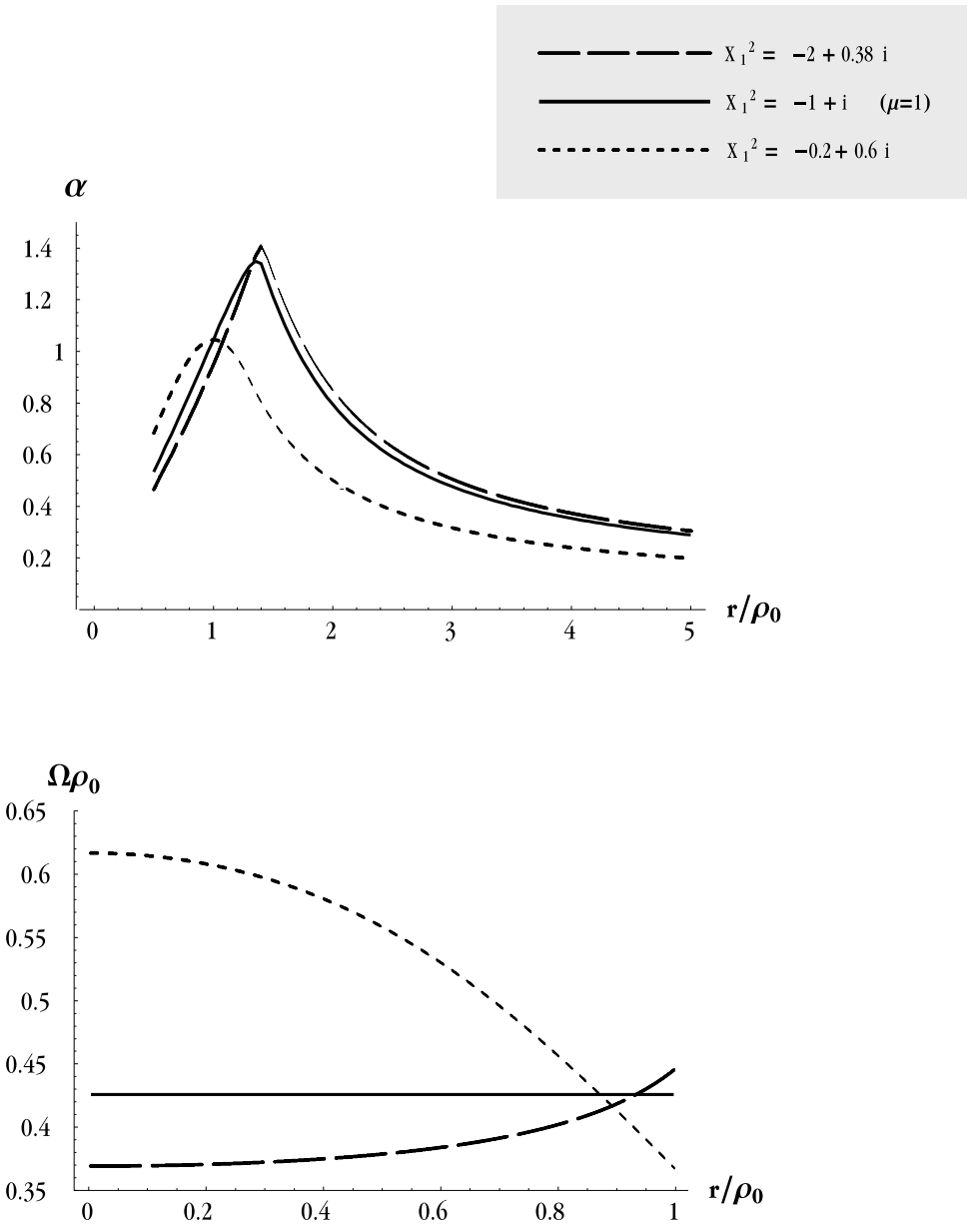

Figure 31: Plot of the deflection angle suffered by light rays (above) due to the gravitational fields of disks with $M^2/J = 18/20$, as a function of the normalised impact parameter. Depicted in the lower of the two plots are the angular velocity profiles of the corresponding disks.

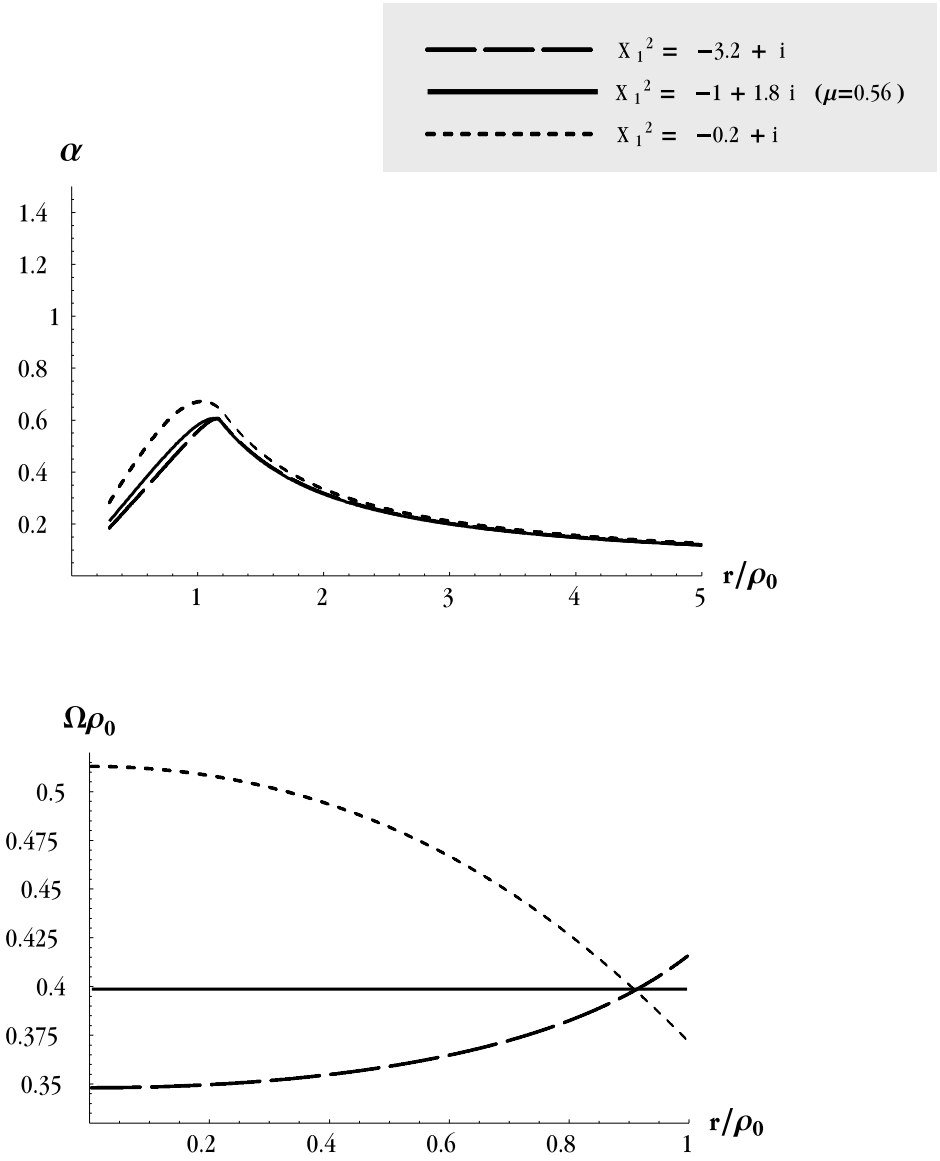

Figure 32: Deflection angle and angular velocity profile for disks with $M^2/J = 11/20$

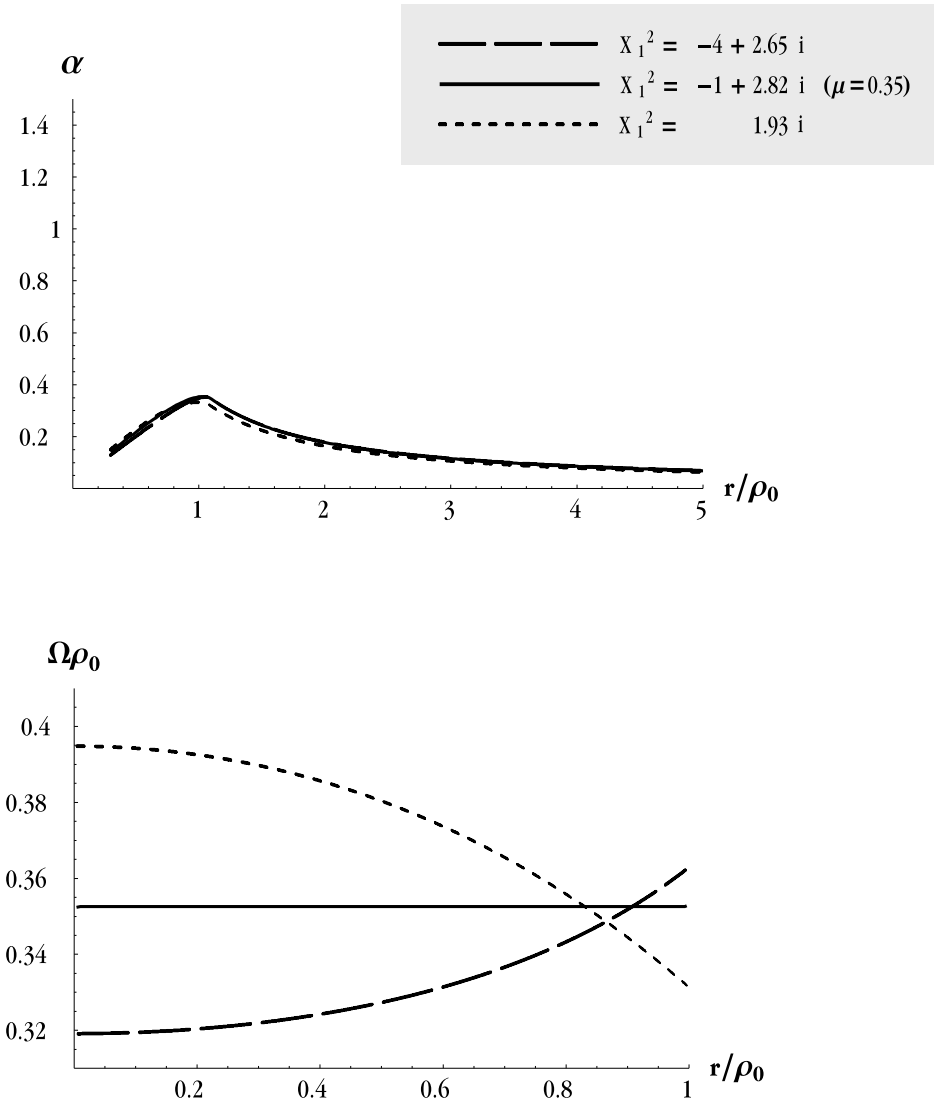

Figure 33: Deflection angle and angular velocity profile for disks with $M^2/J = 9/20$

5 The Lensing Nature of Rigidly Rotating Dust Disks

5.1 Caustic Surfaces and Standard Lensing Theory

The ability of gravitational fields to bend light rays makes them somewhat similar to the common optical lenses used in telescopes and glasses. The main difference between these optical lenses and gravitational 'lenses' is that the deflection caused by a typical linear (spherical convex) optical lens increases with the impact parameter (distance separating the ray from the optical axis in the plane perpendicular to the axis and passing through the centre of the lens) whereas the deflection suffered by a light ray under the influence of a gravitational lens decreases with impact parameter (to a good first order approximation according to $1/r$ as in equation 33). In order to model such behaviour by a glass lens one could use a lens shaped like the bottom of a wine glass[33] as seen in figure 34

The curvature of spacetime in the vicinity of gravitational fields allows the possibility for several light rays to be emitted by a light source and arrive at the eye of an observer, as illustrated in figure 35. The special surface separating regions where the image multiplicity changes suddenly is called the 'caustic surface'.[34] In figure 35 the observer, lens, and source at S_1 are sufficiently well aligned to produce multiple images but for S_2 are not.

There are mathematical proofs (see below) which under plausible assumptions prove that the number of images of a transparent lens is always odd and this number changes by two if and only if the source crosses a caustic. This proposition can be made intuitively very tangible by appealing to the wavefront representation of a typical lensing scenario[35]

[33] see [21]

[34] There is an increasing convention in the literature to (ab)use the term 'caustic' (as will be done in this thesis) to denote the points separating different image multiplicity regions as moved through by a light source for a constant observer (and lens) position. The more accurate term is 'conjugate caustic', the term 'caustic' being reserved for the corresponding positions the observer can move through for fixed source (and lens) positions. It has become customary to investigate the conjugate caustic surface rather than the caustic surface but to drop the word 'conjugate'.

[35] See [22] and [27].

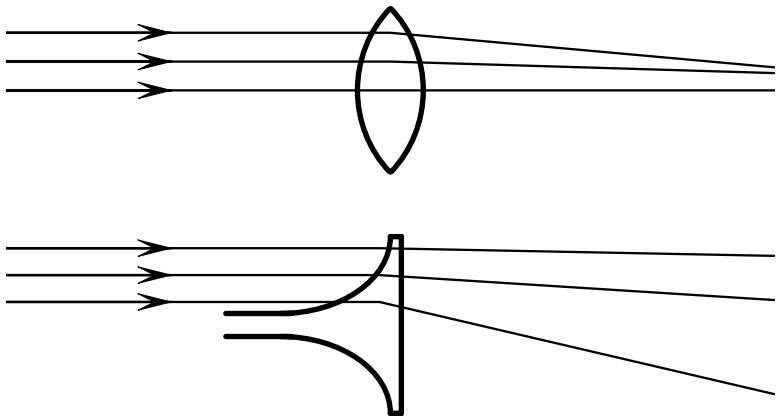

Figure 34: Light rays are bent by typical convex lens (top) increasingly as the impact parameter (distance from the optical axis) increases. This behaviour is what makes it possible for light rays incoming parallel to the optical axis to be focused to a single point (not shown)...the focal point. In contrast, an optical lens in the shape of the bottom of a wine glass bends light rays decreasingly as the impact parameter increases. This is illustrative of the behaviour of a gravitational lens, which has as a result no clearly defined focal point. It does however have something analogous; a special surface... a so called 'caustic surface' (see below). For this analogy to hold strictly for a point mass, one would need to consider the stem of the wine glass to be infinitely long.

as in figure 36. Orthogonal to the wavefronts are the corresponding lightrays. Observers located inside the caustic surface experience each wavefront (and thus the corresponding 'image' producing lightray) three times, whereas those outside see only one image of the source S. As an observer crosses the caustic two of the images converge (the corresponding portions of the wavefront become parallel) and then disappear. As can also be shown mathematically (see below) images close to the caustic appear very bright, and are thus easier to observe in the night sky. The images of extended bodies can also be very distorted yielding some of the most spectacular and beautiful astrophysical images such as the radio ring MG1131+0456 discovered by Hewitt et al. (see Appendix).

Lensing theorists are confident that lenses with elliptical symmetry are excellent models

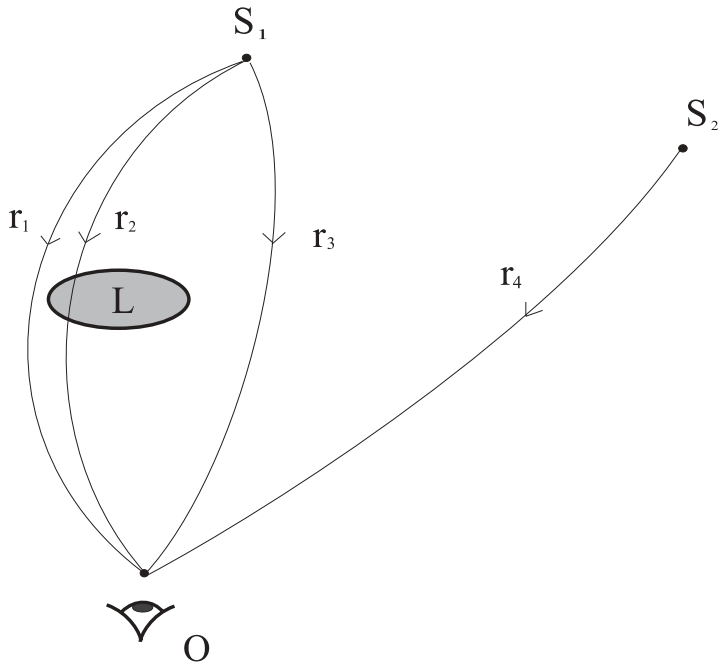

Figure 35: A light source located at position S_1 produces three images corresponding to the three (curved) light rays r_1, r_2 and r_3, as seen by an observer O. When the source migrates to the position S_1 however, it produces only one image corresponding to the single ray r_4. Thus there is a certain special position (in general a surface) separating S_1 and S_2 where the image multiplicity changes abruptly. This is the caustic surface associated with every lens (and observer position).

for most of the observed lensing phenomena to date.[36] To get an impression of the behaviour of the images of such a lens as a function of the source position consider the diagrams[37] figures 38 and 39. The source and lens planes are those planes orthogonal to the line of sight of observer to the centre of the lens containing the light source and lens centre respectively. The critical curves are the curves in the lens plane (the apparent positions of the light source) corresponding to the caustic curves. In general one can consider lensing to be a mapping of apparent (image) positions in the lens plane to true (source) positions in the source plane. In this treatment the caustic curves are then the images of the critical curves under the so-called 'lens mapping'.

[36] see e.g. [25] for a discussion.

[37] see [23]

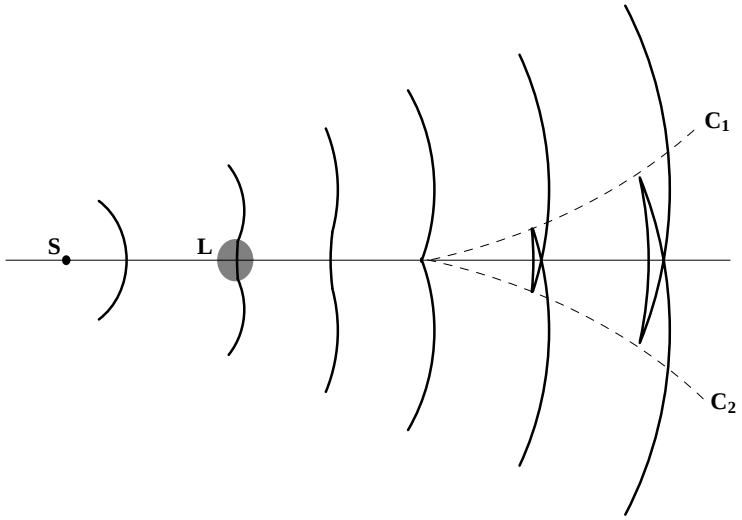

Figure 36: A light source S emits spherical waves which become deformed by the gravitating influence of the lens L. The lens is transparent and thus does not tear the wavefronts but instead causes them to fold back on themselves and dividing space(time) into two regions: those inside the caustic surface (dotted lines) and those outside. The caustic surface forms an envelope of the lightrays.

Knowledge of the caustic surface of lens is crucial to understanding its lensing properties, and tantamount to knowing its qualitative behaviour as a lens, (analogous to knowing all turning points of a smooth, continuous function). Although in general quite complicated, the shape of the caustic surface can be considered to be composed of fundamental building blocks called 'elementary catastrophes'.[38]

Illustrated in figure 37 is the basic geometry of a lensing situation.[39] When lens, source and observer are collinear, the symmetry of the configuration leads to the observer perceiving the light source to be a circle. This circle is the famous 'Einstein ring'. One can get a good estimate of the conditions under which lensing effects become pronounced, by combining

[38]For a nice introduction to catastrophe theory see [24]

[39]In a cosmological background distances here need careful consideration, where they are usually defined as 'angular diameter distances' (see e.g. [12] and [28]). In the case of the Neugebauer-Meinel solution however, the metric (which is asymptotically flat) is explicitly given.

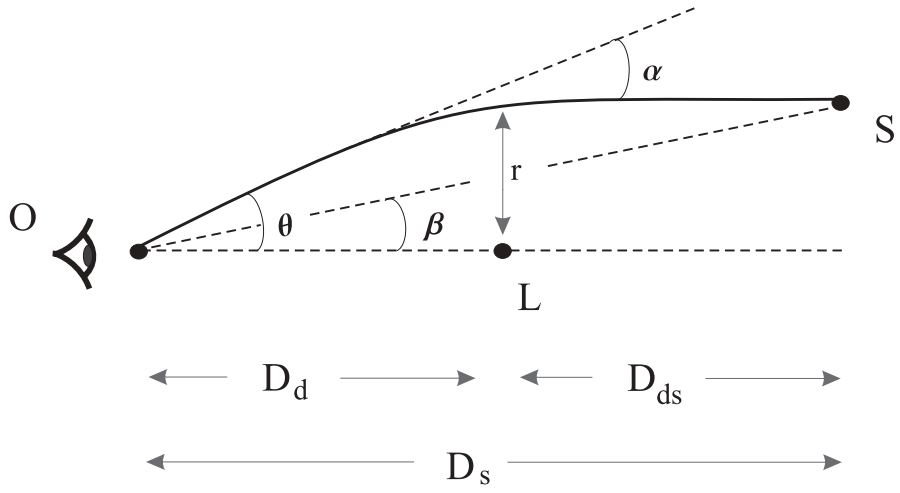

Figure 37: The basic geometry of a lensing scenario. A light ray from a source S located at angle β, gets deflected through an angle α due to the gravitating object which is centred on L. The direction of incidence of the ray at the the observer O, makes it appear that the source is located at angle θ. The angles β and θ are called the 'true position' and 'apparent position', respectively.

figure 37 with equation 33, which can then be written

$$\alpha = \sqrt{\frac{4GMD_{ds}}{c^2 D_d D_s}} \tag{54}$$

Using typical astrophysical data for the variables M and D_d one can estimate the radius of the corresponding Einstein ring, the so-called 'Einstein radius', which can serve as a measure of the typical image separation under such conditions. Only lensing scenarios where the Einstein ring is greater than the maximum physical resolution of modern telescopes should be considered observable, and in this sense astrophysically relevant.

Taking for example, $M = M_\odot$ (solar mass), and $D_{ds} \simeq D_s \gg D_d = 10^4$ light years, equation 54 yields $\alpha_E \simeq 8 \times 10^{-9}$ radians for the Einstein radius, which is beyond the resolution of present day telescopes.Thus one would not generally expect lensing from individual stars to be observable.[40] Using instead data characteristic of lensing due to galaxies, $M = 10^{11} M_\odot$ and $D_d = 10^{10}$ yields $\alpha_E \simeq 2.5 \times 10^{-5}$ radians which is well

[40] An exception to this is the phenomenon of 'microlensing', where individual stars comprising a galactic mass distribution, for example, superimpose their individual deflections on the deflection due to the galaxy as a whole, leading to time dependent intensity fluctuations in the images. This topic will not be discussed here. See [12] for further details.

within the limit of radio telescopes. This makes the study of the lensing properties of the Neugebauer-Meinel disk, as very good first approximation to a galaxy, particularly interesting.[41]

From the basic lensing geometry as indicated in figure 37 one can deduce the so-called 'Lens Equation', also known as the 'Ray-Trace Equation'.

$$\boldsymbol{\eta} = \frac{D_s}{D_d}\boldsymbol{r} - D_{ds}\boldsymbol{\alpha}(\boldsymbol{r}) \tag{55}$$

Here $\boldsymbol{r}$ is as usual the impact vector, which is confined to the plane through the centre of the lens perpendicular to the line joining the observer and the centre of the lens, $\boldsymbol{\theta} = \boldsymbol{r}/D_d$ and $\boldsymbol{\eta} = D_{ds}\boldsymbol{\beta}$, where $\boldsymbol{\beta}$ is the unlensed angular position of the source. Consideration of this equation reveals insight into why astrophysicists hope to use gravitational lensing and careful observations of lensing incidents as a tool in determining much information about the cosmos including strong restrictions on the value of the Hubble constant H, which is a measure of the speed of the expansion of the universe. For example, suppose one knows details such as the lens mass distribution, and the (true) positions of the lens and light source. (There are many possibilities for deducing such quantities such as observation of the relative time delay of light producing the multiple images which may be observable due to intrinsic intensity fluctuations of the source, the relative cosmological redshift of these images inferable from the measured frequency distributions etc.). One can under some general assumptions about the universe (e.g. the average smoothness and density of the mass of the universe[42]), via the distances D_d, D_s and D_{ds} appearing in equation 55, in principle[43], determine the value of H. Conversely, knowledge of the background spacetime (generally through suppositions about Walker-Robertson geometry and results of independent astrophysical observations) allow one to use observations of images to calculate properties of the lens or source.

[41] Any objections to the rigid rotation ansatz of this solution can be to a large extent allayed by the comparisons which were carried out with the Ansorg-Meinel differentially rotating disks (see for example Chapter 3), where this restriction would appear to cause only minor sacrifices in the realistic modelling of a rotating dust disk (galaxy), especially for moderate values of the relativistic parameter, μ.

[42] see [12] for details

[43] of course many practical problems such as the limitations of modern telescopes, interstellar dust obscuring images, incomplete knowledge of some necessary parameters entering the calculations etc. limit the accuracy and usefulness of the results.

Many astrophysical lensing situations which are of interest involve thin (in the direction of the line connecting the earth with the centre of the lens), nearly stationary matter distributions which produce weak gravitational fields. For such thin lenses one projects the matter distribution onto the lens plane and considers the net deflection suffered by an ingoing ray to be the superposition of deflection angles caused by the infinitesimal mass elements of the matter distribution. Thus the total deflection can be represented as an integral over the projected two dimensional matter distribution, of Schwarzschild deflections.

$$\boldsymbol{\alpha}(\boldsymbol{r}) = \frac{4G}{c^2} \int \Sigma(\boldsymbol{r'}) \frac{\boldsymbol{r} - \boldsymbol{r'}}{|\boldsymbol{r} - \boldsymbol{r'}|^2} d^2\boldsymbol{r'} \tag{56}$$

Equation 56 substituted into equation 55 forms one of the cornerstones of standard lensing theory. As previously mentioned, matter distributions with an elliptical projected mass distribution Σ, provide one of the best models for observations. The fact that the projected mass distribution of a disk onto the lens plane is also an ellipse is another good reason for studying the Neugebauer-Meinel solution as a gravitational lens. When source and observer are located far from the lens as is typical, light rays suffer no (non cosmological) frequency shift due to the lens since they lose as much energy falling into the potential well of the lens as they gain climbing out on the other side, and so the surface brightness remains unchanged. The magnification μ_m, of an image can thus be defined as the ratio of the solid angle $\Delta\omega$, the image subtends at the observer, to the solid angle $(\Delta\omega)_0$, the source would subtend in the absence of lensing.

$$\mu_m = \frac{\Delta\omega}{(\Delta\omega)_0} \tag{57}$$

One can consider equation 56 to be a map from the lens plane to the source plane, the so-called 'lens mapping', characterised by the Jacobian matrix

$$\frac{\partial \boldsymbol{\eta}}{\partial \boldsymbol{r}} = \frac{\partial \eta_i}{\partial r_j} \qquad\qquad (i, j = 1, 2) \tag{58}$$

and re-express the magnification as the (absolute value of the) determinant of this mapping

$$\mu_m = \left| \det \frac{\partial \boldsymbol{\eta}}{\partial \boldsymbol{r}} \right|^{-1} \tag{59}$$

It is now possible to define mathematically critical curves as those curves in the lens plane separating regions in which the Jacobian determinant has opposite sign and on

which it vanishes. They are thus curves on which the magnification (formally) diverges.[44] The corresponding curves in the source plane related to the critical curves by the lens mapping 55 are defined to be the critical curves. This mathematical description is fully equivalent to and makes concrete, the intuitive picture given above of the caustic surface as those special positions which when crossed by the source result in images which fuse intensely and disappear. The mathematical concretion of the intuitive idea expressed by figure 36 above can be found in the (again valid under astrophysically very reasonable circumstances; see [12]) *Odd-Number Theorem*, which states that for any transparent mass distribution with finite total mass and with a weak gravitational field produces an odd number of images, except for special source positions. One can understand the result of this theorem as a direct consequence of the fact that image pairs merge and disappear on critical curves. This 'odd image' is the image that must then be left after the source and lens have become so misaligned with the observer that no more light deflection (of those rays reaching the observer's eye) takes place, and it then coincides with the true source position. A further theorem of interest in lensing theory is the *Magnification Theorem*, which states that among the images of any point source produced by an arbitrary transparent matter distribution, that there is always one which is at least as bright as the unlensed source. The field of gravitational lensing traces its roots back to the pioneering work of Einstein [31] and Zwicky [32],[33].

[44]This divergence is in fact a very large *finite* magnification when other subtleties such as the finite size of the source and wave optics are taken into account.

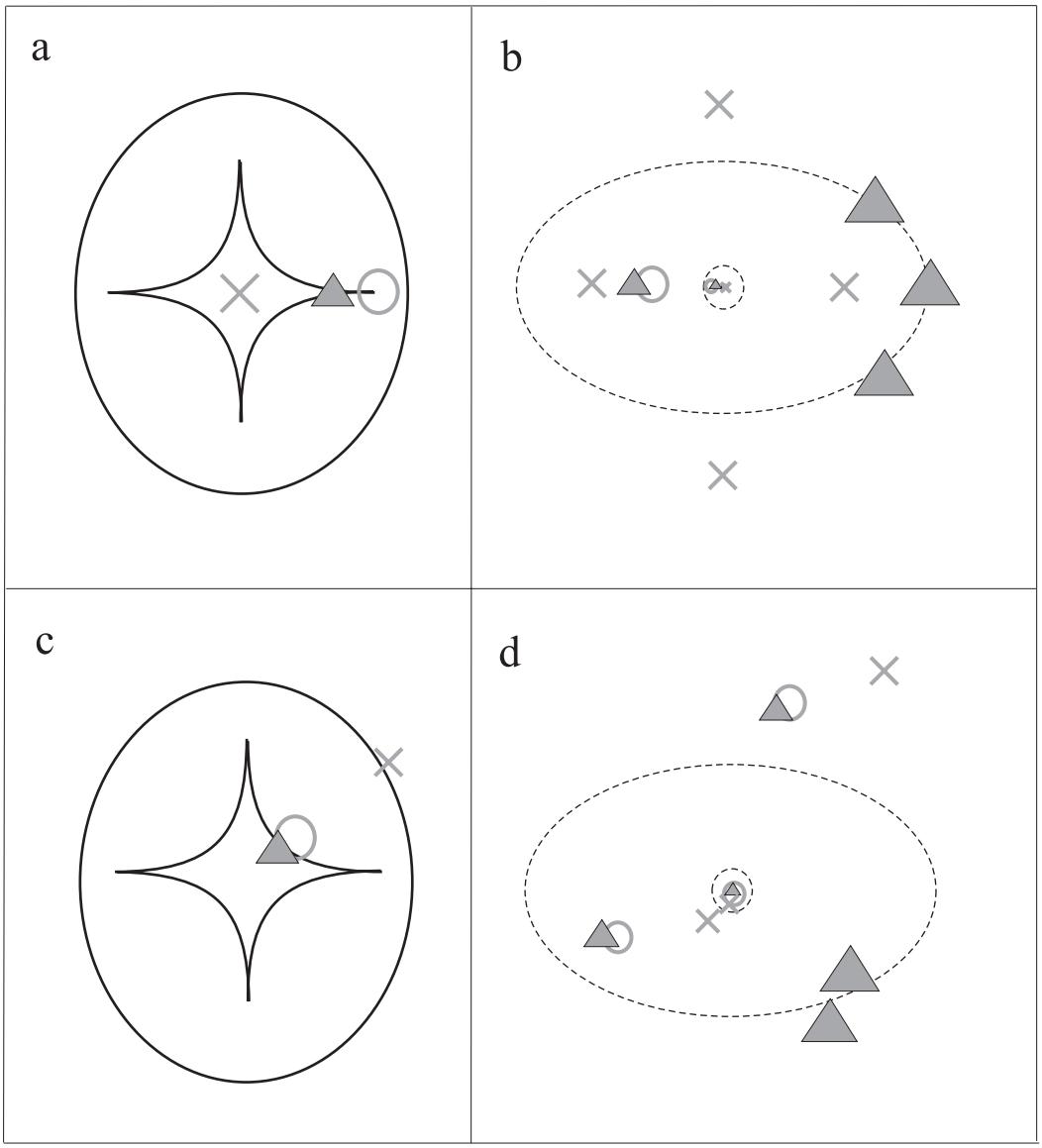

Figure 38: A cross section, in the source plane, of the caustic surface of a generic elliptical lens (a and c), and the corresponding critical curves in the lens plane (b and d). Also shown are some pointlike sources (represented by the cross, filled triangle and circle) and their image positions. The relative sizes of the image symbols in the lens plane indicates the magnification of the respective images. The positions of the crosses in b should be compared to the (Einstein cross) image observed by Macchetto and shown in the Appendix.

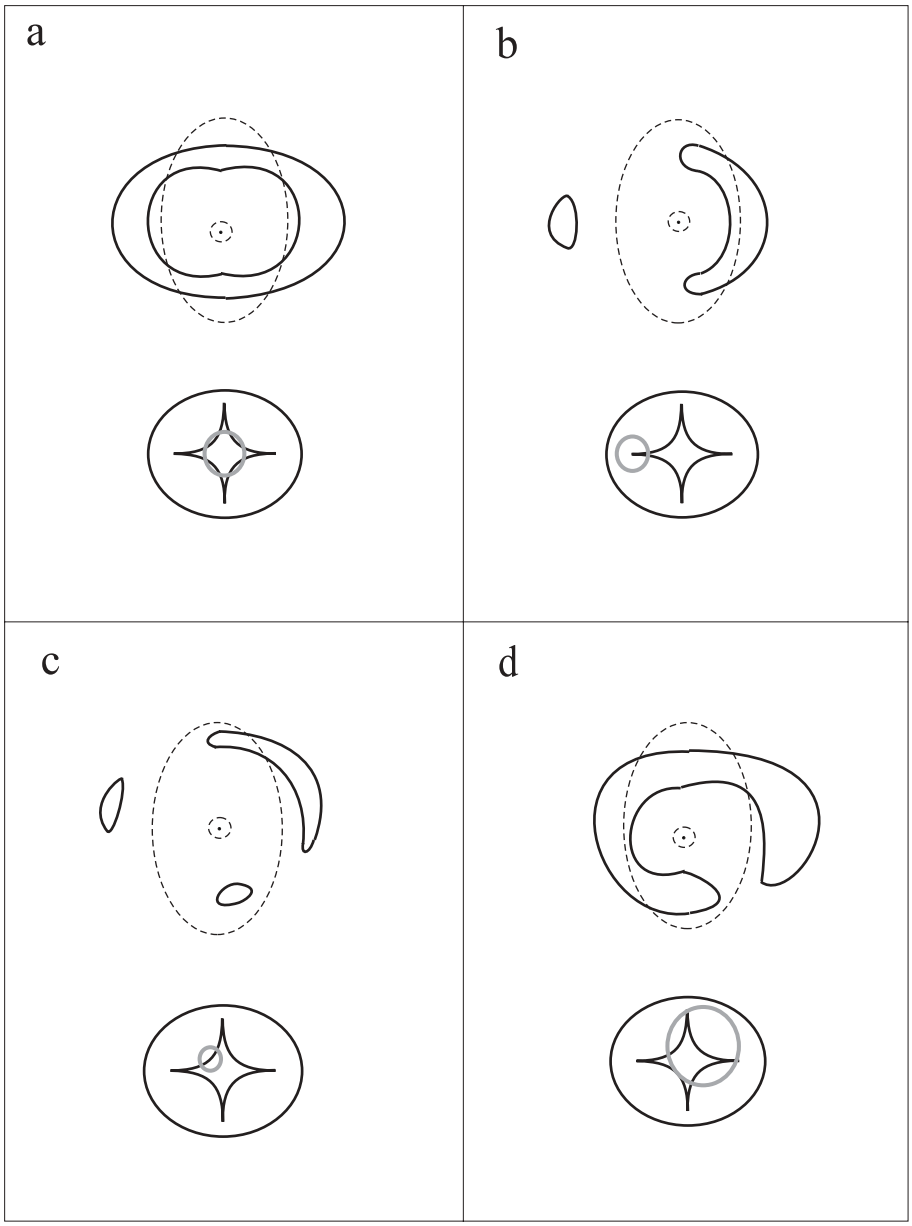

Figure 39: Four cross sections, in the source plane, of the caustic surface of a generic elliptical lens, and the corresponding critical curves in the lens plane. Also shown are some extended sources (circles) and their image positions. The extended and arclike images are typical of the pattern of many observed lensing phenomena. In particular an extended arc in d has been observed by Hewitt et al. in the spectacular MG1131+0456 (see Appendix and [26]).

5.2 Numerical Studies of the Caustic Structure of the Disk

In calculating the caustic structure of the Neugebauer-Meinel disk, the availability of the explicit solution makes it possible to completely sidestep having to use equations 55 and 56, since one can numerically[45] integrate the geodesic equations directly from the lens plane to the source plane. This allows the evaluation of the location of the caustics for a much more relativistic lens than the weak gravitational fields of standard lensing theory and also permits the explicit inclusion of the effects of lens rotation, which are otherwise largely ignored in the literature. Implementation of this method requires the specification of an observer location relative to whom the caustics should be calculated.

5.2.1 Caustics for an arbitrarily located Observer

The method used here is based on an algorithm sketched in [12]. A regular grid G_l, in the lens plane is mapped onto the (irregular) grid G_l', in the source plane. This mapping is carried out for a given observer position O, by using this as a starting point for the light rays, which are interpolated through each node of the grid G_l to the lens plane in order to locate the corresponding node of the grid G_l'. A regular grid G_s, in the source plane is then compared to G_l' in order to locate the caustics. To this end each node of G_s is checked to see which triangles (composed of adjacent nodes) of the grid G_l have image triangles (in G_l') which contain the node of G_s in question. Thus each node of G_s can be allocated an integer m, representing the number of 'source triangles' inside which it is contained.[46] Those nodes of G_s which have adjacent nodes with an m value which differs by 2 (recall images fuse in pairs) or a multiple of 2, are located near a caustic. The resolution of the caustic obtained by this procedure is determined by the spacing of the grid nodes. The three dimensional caustic surface is obtained by varying the position

[45] It should be noted that although equations 55 and 56 give an explicit expression for the lens mapping, they also still require numerical solution for all but the simplest mass distributions.

[46] Triangles are a better choice than for example rectangles, since triangles are in general mapped onto triangles in the source plane but rectangles are in general not mapped onto rectangles but non-convex shapes in the source plane. Containment within a triangle is simpler to evaluate than containment within the (non-convex) image of a rectangle

of the source plane. (This is in practice of course done by using several source planes to start with, thus requiring only one set of integrations of the geodesic equations for each observer position).

Consider the grid shown in figure 40 for an axial observer. The central dark disk-like region is one where the image multiplicity of sources located here is three. Its boundary marks the caustic surface and the corresponding nodes in the grid G_l mark the critical curve. Illustration of the sudden decrease of image multiplicity by exactly two can be seen in figure 41. Movement of the observer away from the symmetry axis induces a sudden qualitative change into the structure of the caustic surface. The single multiple (3) image region visible in figure 40 degenerates into 2 multiple image regions, the inner one corresponding to image multiplicities of 5, and the outer to image multiplicities of 3. Also interesting is the shape of the resulting caustics which are in striking agreement with those calculated by Blandford et al. for a lens with elliptical symmetry (see figures 38 and 39); the caustic surface of a disk relative to an observer away from the axis turns out to be qualitatively similar to that produced by an elliptical mass distribution for moderate gravitational fields. As the value of μ is increased the symmetry of the caustic degenerates and particularly noticeable is the lateral shifting of the diamond shaped inner caustic which becomes increasingly distorted. This behaviour is a consequence of the increasingly strong influence of the rotation of the disk, a factor which is not considered in standard lensing theory embodied by such equations as 55 and 56.

A thorough examination of the caustic surfaces of the rotating disk for non-axial observers using the method described above is numerically very intensive and well beyond the computing power of a typical PC or workstation. Apart from the significant task of numerically integrating all geodesics, the main limiting factor is the checking of each node of the grid G_s for containment within each triangle of the grid G'_l. For each node of G_s and each triangle of G'_l this requires 9 floating point operations (the computation involves the calculation of three cross products). Thus the number n, of floating point operations involved in just this checking for a single cross section of the caustic surface using a grid of dimension p, increases exponentially with p. For example using a very moderate grid with dimension $n = 100$, this involves 10^9 floating point operations. This

number then needs to be multiplied by the number of source planes (also of the order of n), the number of observer positions, and the number of values of the relativistic parameter μ, under consideration. Such a task is only suited to implementation on a large parallel computer and is an interesting possibility for future work. The results given here still give good insight into those that could be expected from such a study. In order to get full use of moderate computing power one should restrict one's attention to observers located on the ζ-axis, which allows implementation of a different algorithm which fully exploits the symmetry of the configuration. This is the topic of the next section.

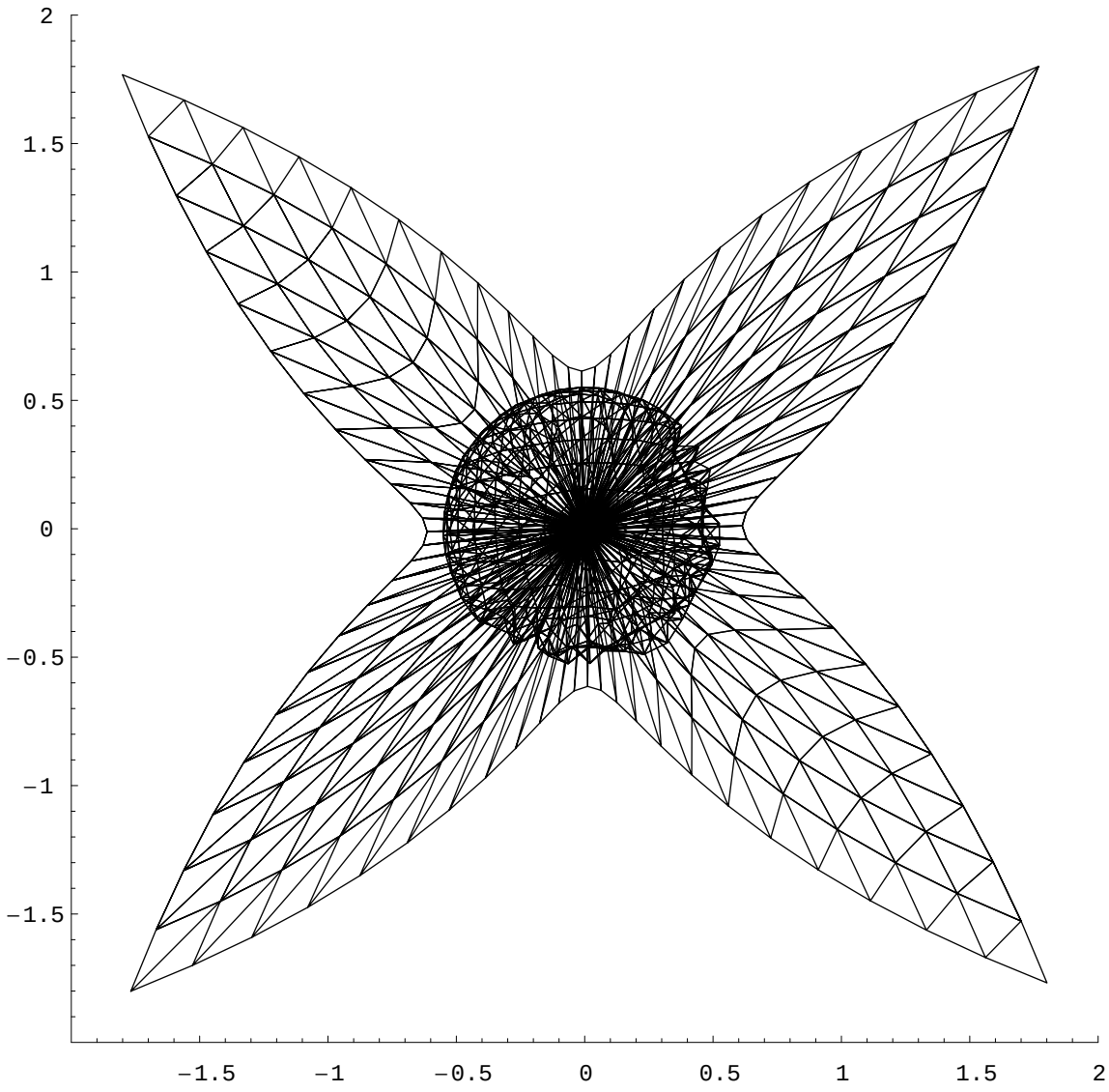

Figure 40: The grid G_l' in the source plane located at $\zeta/\rho_0 = -15$ which is the image of a regular (rectangular) grid G_l, in the lens plane ($\zeta/\rho_0 = 0$), which is constructed by mapping the nodes of G_l along the light rays to the source plane, from the position of an observer located on the disk's symmetry axis at $\zeta/\rho_0 = 10$ with $\mu = 0.2$. In the process the grid folds over on itself, equivalent to the folding of the wavefronts illustrated in figure 36. The dark disk-shaped region in the centre is the locus of source positions which produce three images, whereas those outside produce only one.

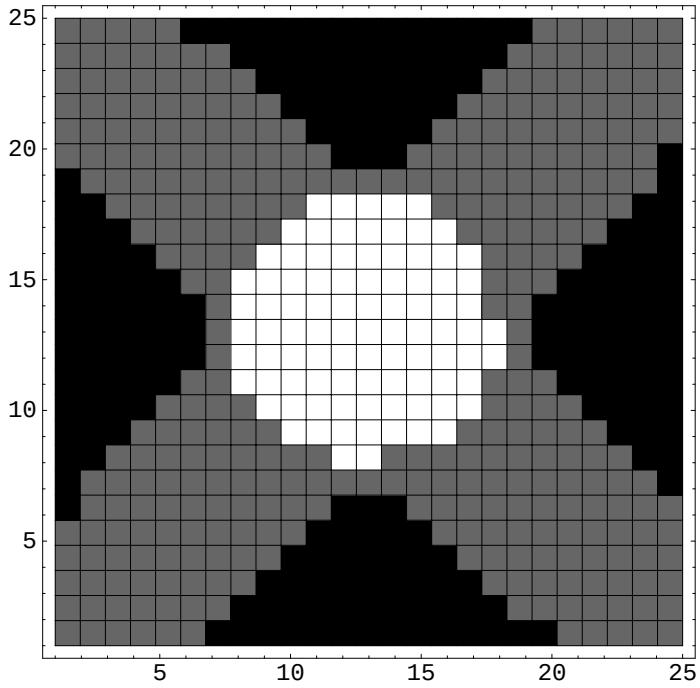

Figure 41: A raster showing the image multiplicity of nodes on the source grid G_s corresponding to figure 40 above. Each of the tiles corresponds to a single node of G_s. The colour of the tiles represents the image multiplicity of the node in question, those in the centre have an image multiplicity of 3 and those (grey) outside having 1. (The black region is simply a consequence of the fact that the grid used was finite in extent, and in reality the region containing nodes with an image multiplicity of 1 would extend indefinitely outward in all directions).

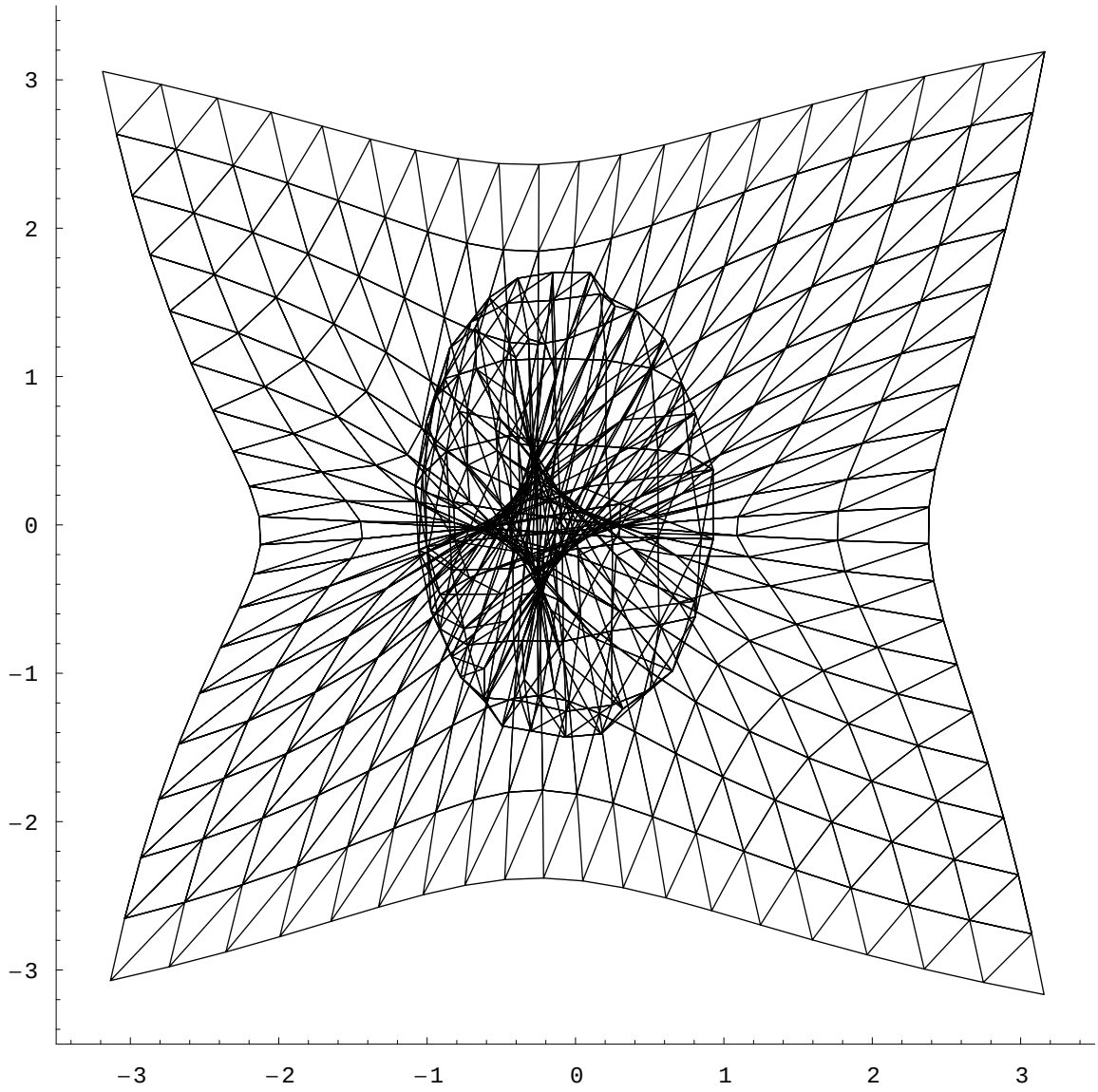

Figure 42: The grid G_l' in the source plane located at $\zeta/\rho_0 = -15$ mapped from an observer situated at $\rho/\rho_0 = \zeta/\rho_0 = 7$, with $\mu = 0.2$.

5.2.2 Caustics for an observer located on the Symmetry Axis

A method which can be employed to calculate the caustic surface relative to an observer located on the symmetry axis of the disk is indicated in figure 43

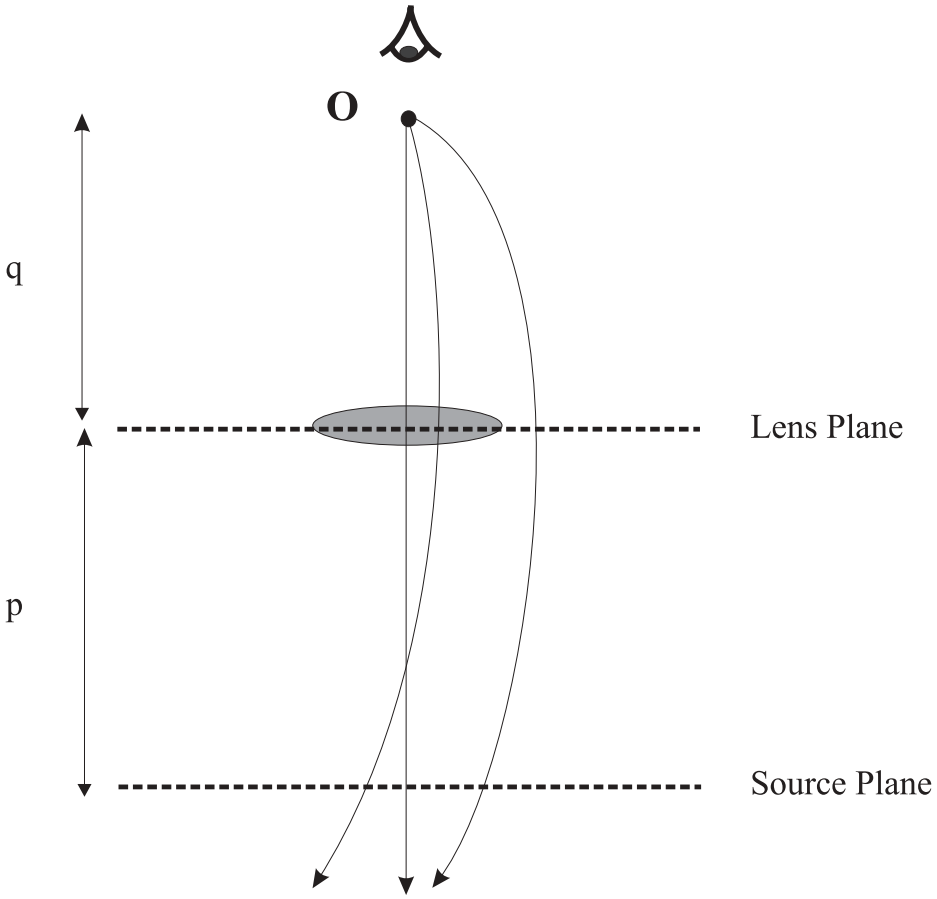

Figure 43: From the observer O, rays are followed back a through the lens plane which is situated a distance q from the O, to the source plane which is located a distance p behind the lens.

The points p_l at which each ray strikes the lens plane, and p_s at which each ray strikes the source plane are recorded. The radial distance[47] ρ_l, from p_l to the centre of the disk,

[47]It is best to plot this radial distance rather than the 2 dimensional coordinates of the intersection point, since this avoids the necessity of having to include the dragging effects of the field in the calculation. The dragging effects cause pairs of images to approach the critical curves along a curved path rather than

and the radial distance ρ_s, from p_s to the symmetry axis can then be plotted as shown in figure 44.

The results of these calculations are shown in figures 45-49, where the radius of the cross section of the (axially symmetric) caustic surface in the plane $\zeta/\rho_0 = p$ is plotted against the observer's location. These results are seen to be in good qualitative agreement with those presented for example in [12] for a homogeneous rigidly rotating disk using the standard lensing equations. Also comparison with figure 40 shows that both methods involved yield good agreement in the prediction of the radius of the cross section of the caustic surface.

radially, but for the symmetric arrangement of lens, source and observer treated here, do not effect the position of the caustic or critical curves which can be expected to be axially symmetric. The final caustic calculated will therefore still be perfectly general.

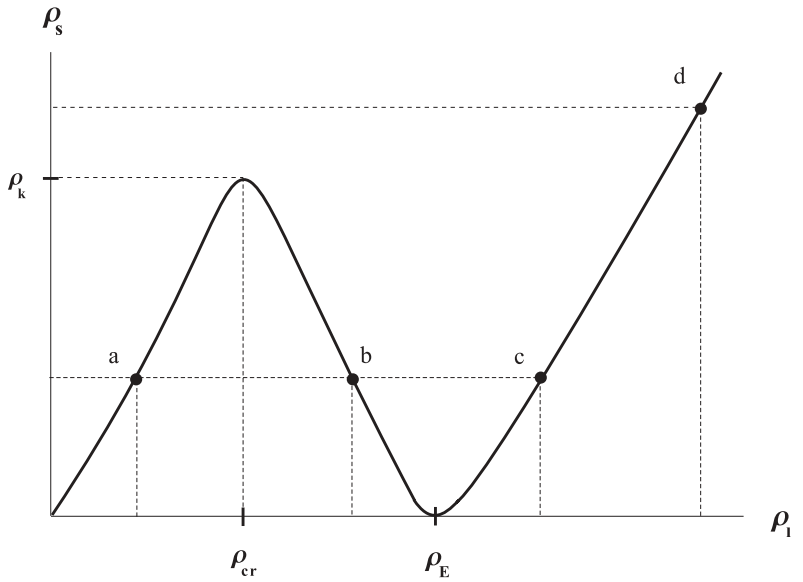

Figure 44: The radial distance from the intersection of the light ray with the ($\zeta = p$) source plane to the axis ρ_s, is plotted against the radial distance from the intersection of the light ray with the ($\zeta = q$) lens plane to the axis, ρ_l. For a typical source position (ρ_s-axis) not far from the axis there will be three (corresponding to a,b and c) image positions (ρ_l-axis). As the source moves radially outward two (corresponding to b and c) of these images fuse and disappear. For source positions outside ρ_k there will be only one (corresponding to d) image in the lens plane. The maximum ρ_k, of the curve marks the radius of the cross section of the caustic surface, and the corresponding value ρ_{cr}, is the radius of the circular critical curve. When the source is also located on the symmetry axis the resulting image is a ring...the famous 'Einstein ring', which has a radius ρ_E.

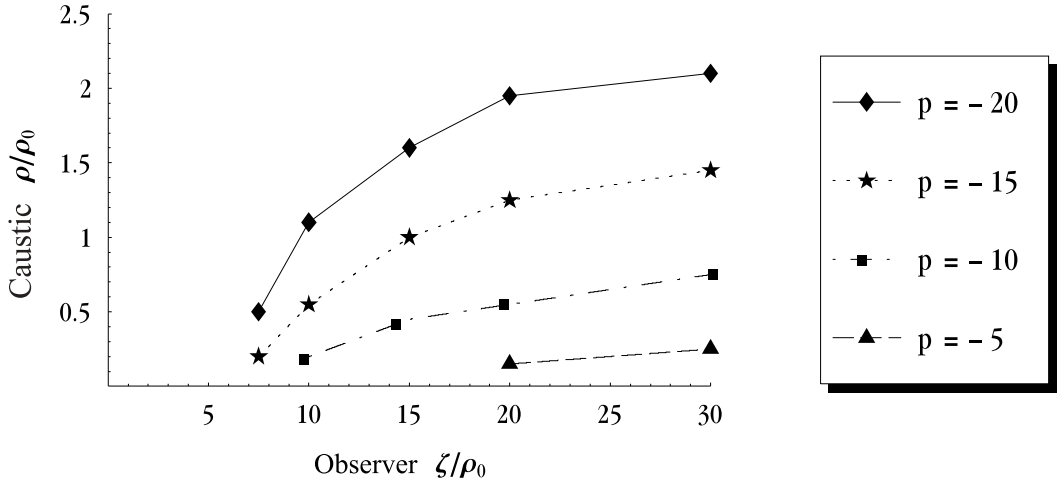

Figure 45: The radius of the cross section of the caustic surface plotted against the observer's location, for various positions of the source plane $\zeta/\rho_0 = \mathrm{p}$ with $\mu = 0.2$

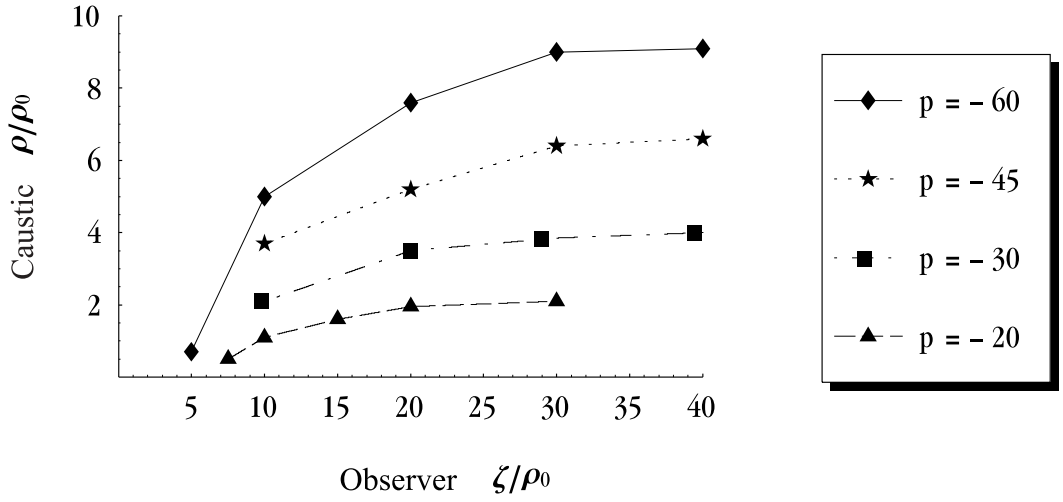

Figure 46: $\mu = 0.2$

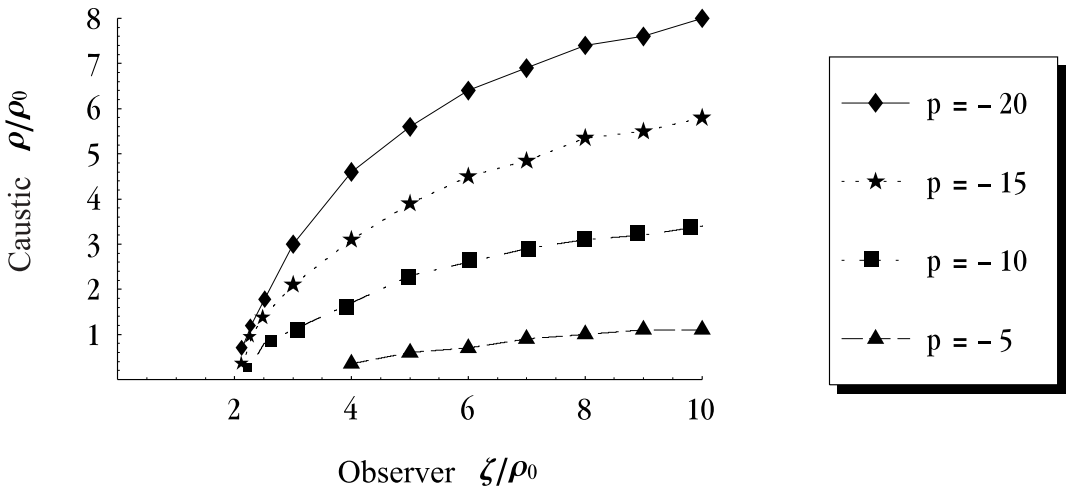

Figure 47: $\mu = 0.5$

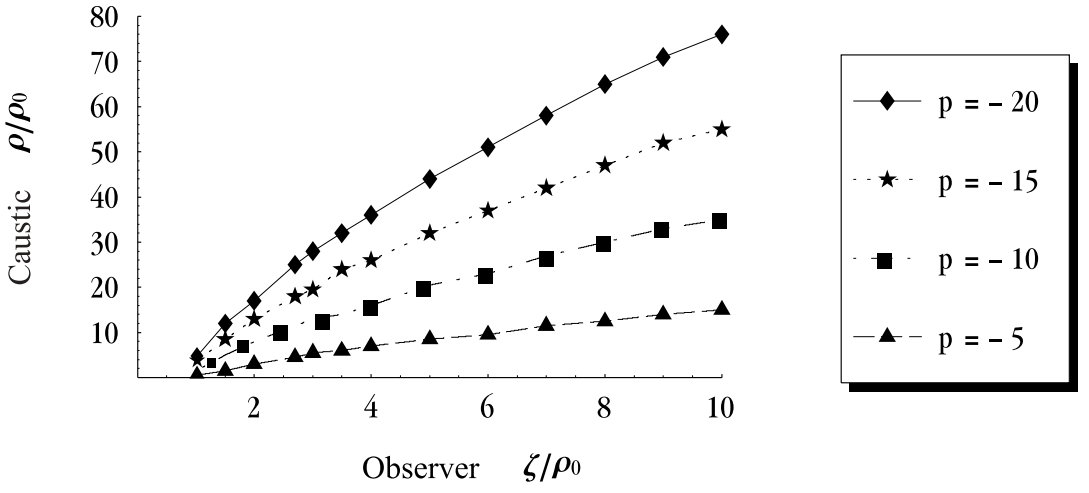

Figure 48: $\mu = 1.0$

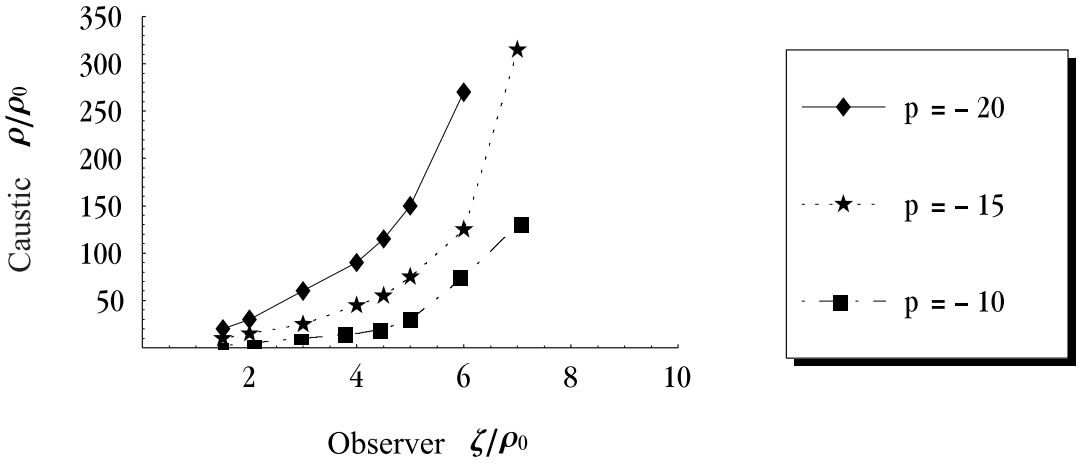

Figure 49: $\mu = 1.1$

6 Summary and Conclusion

By far the single greatest source of information, both direct and indirect, afforded to astrophysicists on the universe in which we live is the light[48] reaching us from the distant heavens. On its journey, this light is influenced by gravitational fields much stronger than those familiar to us on the earth. The more distant the source of light the more important it is to take into consideration these gravitational effects since not only are such effects all the more likely to accumulate but also because the more distant the source, the further back in time the light in question permits us to look into the history of the cosmos. One of the most important sources of such perturbing influences on light rays are galaxies, and the best relativistic description of galaxies available to physicists is the Neugebauer-Meinel solution of Einstein's field equations. Using primarily this solution, investigations have been undertaken to study the gravitational influences on light rays from three different viewpoints.

Firstly, the visual appearance of the rotating disk has been calculated including the redshift of the photons involved, which proved among other things to be instructive of just how extreme the effects of strong gravitational fields on light can be. Particularly interesting was the fact that due to the bending of light rays, one could simultaneously see the upper and lower sides of the disk. Indeed, for sufficiently high values of the relativistic parameter μ, it was even possible to see several times around the disk via the higher order light rays. An appropriate choice of the surface pattern used, enables one to separate the effects of the finite speed of light from those due only to the gravitational field. Secondly, efforts were concentrated on individual rays and calculation of the angle through which they become deflected. To this end, explicit formulae were derived using the Kopeikin-Schäfer theory of light propagation, for the radial (zeroth order) and the tangential (first order) deflections. Comparisons were also made between results obtained using the Neugebauer-Meinel solution and those obtained from the Ansorg-Meinel solution, which illustrated at what value of the relativistic parameter μ, one could expect the

[48] In the title and throughout this thesis the term 'light' has been used, but all considerations and results presented apply equally well to the other forms of electromagnetic radiation including radio waves.

rigid rotation ansatz to be significant. Thirdly, the lensing nature of the rigidly rotating disk was investigated, and in particular the caustic structure. Such study is particularly useful as a testbed for some of the models of standard lensing theory (in particular the elliptical lens models) which are unfortunately limited in their validity to weak fields. Use of the Neugebauer-Meinel solution to directly integrate the geodesic equations enables one to sidestep these approximations and weak field limitations, permitting an impression of more extreme gravitational lensing and thus a better impression of the point at which such models in the standard theory deviate from a more accurate relativistic description, including in particular the effects of rotation.

A The Function $V_0(\mu)$

The function $V_0(\mu)$ appearing in equation 13 can be given explicitly as follows

$$V_0(\mu) = -\frac{1}{2}\sinh^{-1}\left\{\mu + \frac{1+\mu^2}{\wp[I(\mu); \frac{4}{3}\mu^2 - 4, \frac{8}{3}\mu(1+\frac{\mu^2}{9})] - \frac{2}{3}\mu}\right\}$$

where the function $I(\mu)$ is given by

$$I(\mu) = \frac{1}{\pi}\int_0^\mu \frac{\ln(x+\sqrt{1+x^2})}{\sqrt{(1+x^2)(\mu-x)}} \quad dx$$

and the Weierstraß function $\wp$ is defined by

$$\int_{\wp(x;g_2,g_3)}^{\infty} \frac{dt}{\sqrt{4t^2 - g_2 t - g_3}} = x.$$

The range of values of the relativistic parameter $0 < \mu < 4.629...$ correspond to the range $0 > V_0 > -\infty$ (with $|V_0| << 1$ corresponding to the Newtonian limit $\mu << 1$).

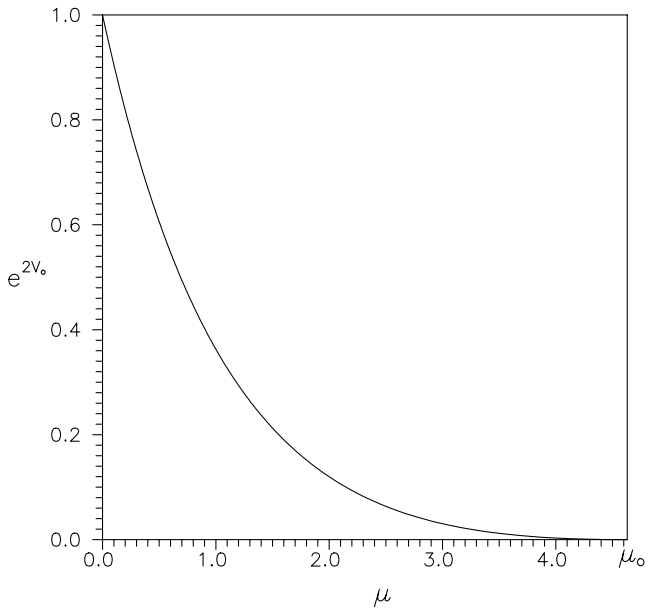

Figure 50: A plot of e^{2V_0} as a function of the relativistic parameter μ.

B Observed Gravitational Lensing Phenomena

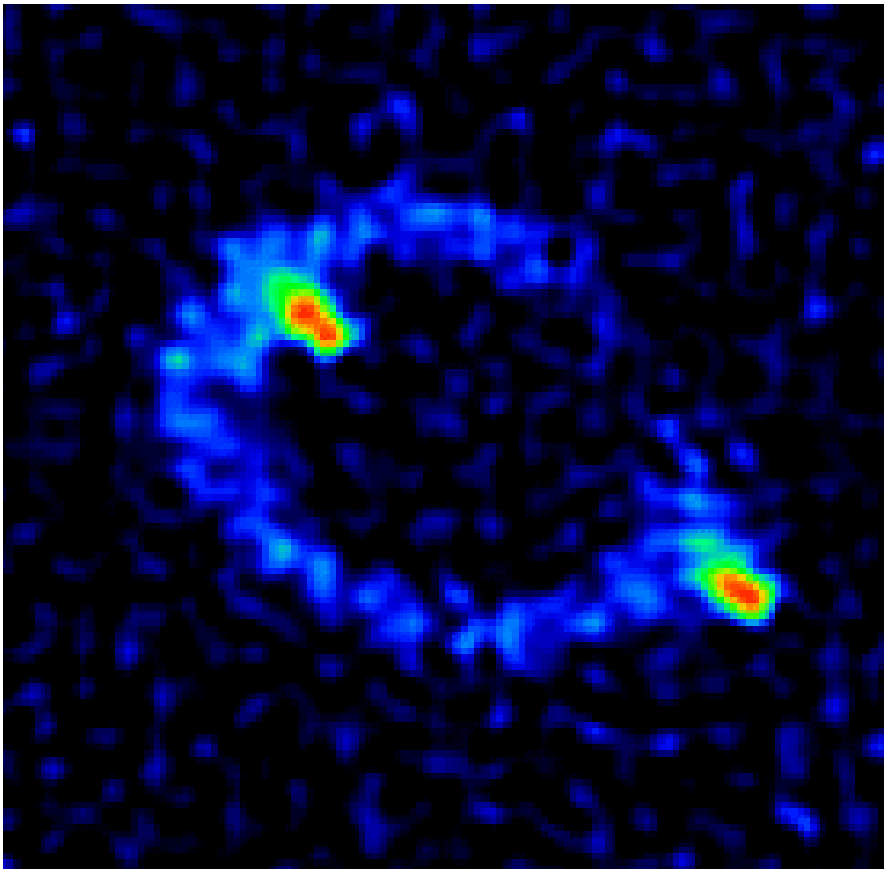

Figure 51: The spectacular MG1131+0456 Einstein ring discovered in 1984 by J. Hewitt et al. as part of the National Radio Astronomy Observatory VLA (Very Large Array) lens search. See eg. [26] and [28] for details. This image should be compared with d in figure 39.

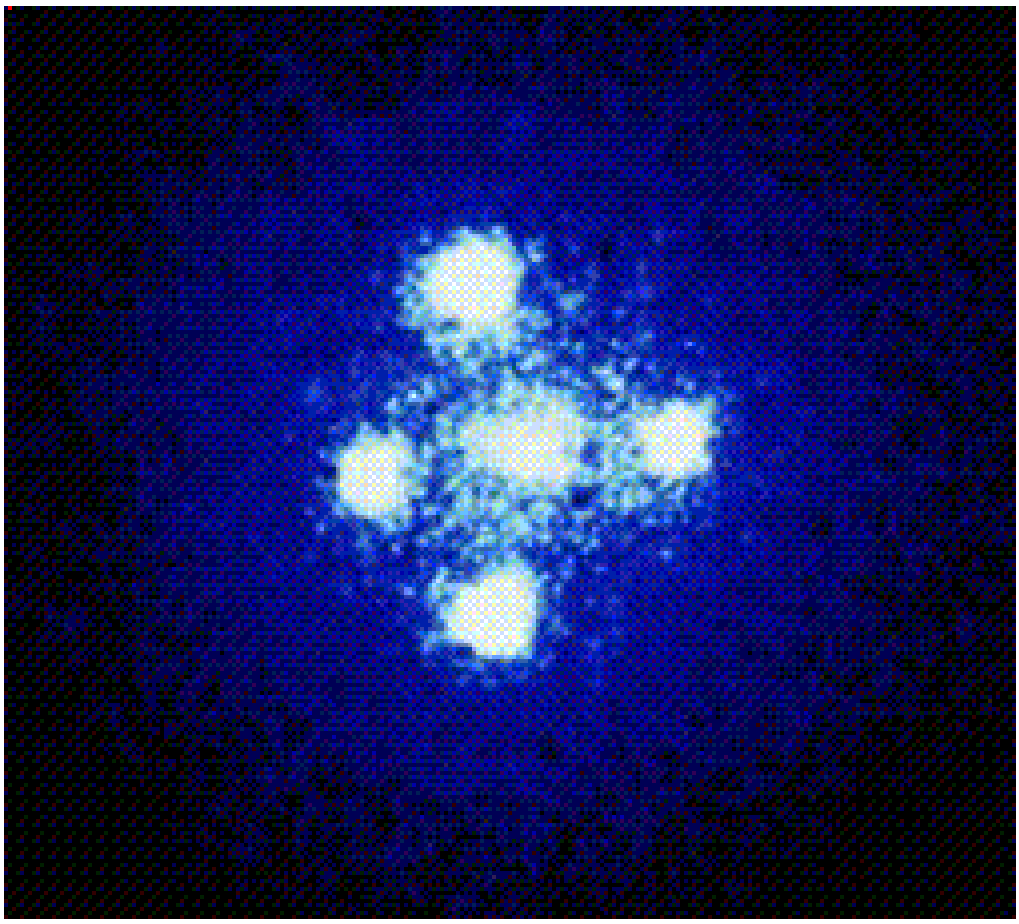

Figure 52: The optical image of Q2237+031, the Einstein cross discovered by F.D.Macchetto using the Hubble Space Telescope. This image should be compared to the positions of the crosses in b of figure 38.

References

[1] Neugebauer, G. and Meinel, R., *General Relativistic Gravitational Field of a Rigidly Rotating Disk of Dust: Axis Potential, Disk Metric, and Surface Mass Density*, 1995, Phys.Rev.Lett. **75**, 3046.

[2] Ansorg, M. and Meinel, R., *Differentially rotating disks of dust*, 1999, Gen.Rel.Grav. (In press).

[3] Ansorg, M, *Zeitartige geodätische Bewegungen im allgemein-relativistischen Gravitionsfeld einer starr rotierenden Staubscheibe*, 1998, Ph.D. Thesis, Friedrich-Schiller-Universität, Jena.

[4] Nollert, H., Kraus, U., and Ruder, H., 1996, *Visualisation in Curved Spacetimes*, in *Relativity and Scientific Computing*, Springer.

[5] Kraus, U., 1998, in *Relativistic Astrophysics*, Vieweg.

[6] Nollert, H., Ruder, H., Herold and H., Kraus, U., 1989 in *Astronomy and Astrophysics*.

[7] Weiskopf, D., *A Texture Mapping Approach for the Visualisation of Special Relativity*, in *IEEE Visualisation 1999, Late Breaking Hot Topics Proceedings*.

[8] Rau, R., Weiskopf, D. and Ruder, H., 1998, *Special Relativity in Virtual Reality* in *Mathematical Visualisation*, Springer-Verlag.

[9] Ansorg, M. and Weiskopf, D., *Visualisation of the General Relativistic Disk Of Dust*, Ann.Phys. (In press).

[10] Kopeikin and Schäfer, 1999, *Lorenz Covariant Theory of Light Propagation in Gravitational Fields of Arbitrary-Moving Bodies*, Phys. Rev., **D60**, 124002.

[11] Wald, Robert M., 1984, *General Relativity*, The University of Chicago Press.

[12] Schneider P., Ehlers J., Falco E.E, 1992, *Gravitational Lenses*, Springer Verlag.

[13] Walsh, D., Carswell, R.F. and Weymann, R.J., 1979, Nature, **279**, 381.

[14] Kleinwächter, A., 1995, *Untersuchungen zu rotierenden Scheiben in der Allgemeinen Relativitätstheorie*, Ph.D. Thesis, Friedrich-Schiller-Universität, Jena.

[15] Bardeen, J. M., and Wagoner, R. V., *Relativistic Disks. I. Uniform Rotation*, 1971, *Astrophys. J.*, **167**, 359.

[16] Weinberg, S., 1972, *Gravitation and Cosmology*, John Wiley & Sons.

[17] Landau, L.D. & Lifschitz, E.M., 1971, *The Classical Theory of Fields*, Pergamon.

[18] Fock, V.A., 1959, *The Theory of Space, Time and Gravitation*, Pergamon Press.

[19] Chandraskehar, S., *Selected Papers, Volume 5, Relativistic Astrophysics*, *Conservation Laws in General Relativity and in the Post-Newtonian Approximations*, University of Chicage Press.

[20] Kley, W. and Schäfer, G., 1994, *Post-Newtonian oscillations of a rotating disk of dust*, Physical Rev. D, Volume 50, Number 10.

[21] Chaffee, Freidrich H. jun, 1989, *Eine Gravitationslinse wird entdeckt*, Gravitation, Spektrum der Wissenschaft.

[22] Ohanian, Hans C. and Ruffini Remo, 1994, *Gravitation and Spacetime*, Norton and Company.

[23] Narayan, Ramesh and Wallington Sylvanie, *Introduction to the Basic Concepts of Gravitational Lensing*, in *Gravitational Lenses ...Proceedings of the Hamburg Conference 1991.*

[24] Arnold, V.I., 1992, *Catastrophe Theory*, Springer-Verlag.

[25] Narayan, R. and Grossman, S., *The Versatile Elliptical Gravitational Lens*, in *Gravitational Lenses*, Proceedings of the Conference held in Cambridge, Massachusetts, USA, 1988, Springer-Verlag

[26] Hewitt, J. N. et al., 1988, *Results of the VLA Gravitational Lens Survey*, in *Gravitational Lenses*, Proceedings of the Conference held in Cambridge, Massachusetts, USA, Springer-Verlag.

[27] Nityananda, R., 1989, *Pictures of Gravitational Lensing*, in *Gravitational Lensing*, Proceedings, Toulouse, France, Springer-Verlag.

[28] Ehlers, J. and Schneider, P., *Gravitational Lensing*, in *Relativistic Gravity Research*, Proceedings, Bad Honnef 1991, Springer-Verlag.

[29] Neugebauer, G., Meinel, R., and Kleinwächter, A., *Relativistically rotating dust*, 1996, Helv.Phys.Acta. **69**, 472.

[30] Neugebauer, G. and Meinel, R., *The Einsteinian Gravitational Field of the Rigidly Rotating Disk of Dust*, 1993, Astrophys. J., **414**, L97.

[31] Einstein, A., 1936, Science, *Lens-like action of a star by the deviation of light in the gravitational field*, **84**, 506.

[32] Zwicky, F., 1937, Phys.Rev., *Nebulae as Gravitational Lenses*, **51**, 290.

[33] Zwicky, F., 1937, Phys.Rev., *On the probability of detecting of Nebulae which act as Gravitational Lenses*, **51**, 679.

Acknowledgements

I am greatly indebted to my supervisor, Prof. Gernot Neugebauer, and to Prof. Reinhard Meinel for all their help, support and advice over the past several years, and to whom I would like to express my deepest gratitude. Warmest thanks also to Prof. Sergei Kopeikin, Prof. Gerhard Schäfer, Thomas Moran, David Petroff and Ruth Heidrich for many helpful discussions and suggestions.

Statement of Originality

I hereby declare that any work of other persons I have made use of in this thesis has been openly and clearly cited either in the bibliography or the main body of the text.

Jena 17.01.2000 Declan Moran.

Curriculum Vitae

19.07.1972	Born in Ballinasloe, Co.Galway, Ireland.
1976-1985	Cloonloo National School, Boyle, Co. Sligo
1985-1990	St. Nathy's College, Ballaghaderreen, Co. Roscommon.
1990-1993	BSc. in Applied Mathematics at University College Galway.
1993-1995	BSc. in Theoretical Physics at the University of Kent at Canterbury, England.
1995-1996	Certificate of Advanced Studies in Mathematics at the University Cambridge, England.
since 1996	Ph.D student at the Friedrich Schiller University, Jena, Germany.

Jena 17.01.2000 Declan Moran.

Thesen zur Dissertation

"Light Rays in the Gravitational Field of Rotating Disks of Dust in General Relativity"

("Lichtstrahlen im Gravitationsfeld rotierender Staubscheiben in der Allgemeinen Relativitätstheorie")

von Declan Moran

1. Mit Hilfe der 'ray-casting' Methode ist es möglich, das optische Erscheinungsbild einer starr rotierenden Staubscheibe zu berechnen und gleichzeitig die gravitative Rotverschiebung sichtbar zu machen. Interessanterweise kann man auf Grund relativistischer Effekte Ober- und Unterseite der Scheibe zugleich sehen. (Die Lichtstrahlen können die Scheibe sogar mehrfach umlaufen!)

2. Die Verwendung geeigneter (gedachter) Muster auf der Oberfläche der Staubscheibe erlaubt es, speziell relativistische Bildverzerrungen (endliche Lichtgeschwindigkeit) von allgemein-relativistischen (Krümmung von Lichtstrahlen) zu unterscheiden.

3. Bei der Lichtablenkung an rotierenden Scheiben tritt zusätzlich zum Einsteinschen Ablenkwinkel ein tangentialer Ablenkwinkel α_t auf. Unter Verwendung der approximativen Kopeikin-Schäfer-Theorie erhält man für einen Lichtstrahl, der die Symmetrieachse der Scheibe im Abstand D von Scheibenzentrum durchquert

   $$\alpha_t = \frac{16\rho_0^5\Omega^3}{15\pi Drc^3}$$

   wobei ρ_0 der Scheibenradius, Ω die Winkelgeschwindigkeit, r der Stoßparameter und c die Lichtgeschwindigkeit sind.

4. Numerisch kann der Verlauf der Lichtstrahlen auch ohne Näherungsannahmen berechnet werden. Dies erlaubt es, die Gültigkeitsgrenzen der Kopeikin-Schäfer-Theorie zu bestimmen. Besonders illustrativ ist hier die Gegenüberstellung von Scheiben mit unterschiedlichen Rotationsgesetzen, deren Ablenkwinkel sich erst für starke Gravitationsfelder signifikant unterscheiden.

5. Die Struktur der Kaustiken der Neugebauer-Meinel-Staubscheibe weicht im ultrarelativistischen Bereich beträchtlich von den auf Näherungsvoraussetzungen beruhenden elliptischen Modellen der Standard-Linsentheorie ab.

6. Der sehr große Rechenaufwand bei der Bestimmung der Kaustiken gestattet es im allgemeinen nicht, eine detaillierte Analyse für alle Beobachterpositionen und alle Werte der Lösungsparameter auf einem Einzelprozessor-Computer vorzunehmen. Hingegen konnte für symmetrische Fälle (Beobachter auf der Symmetrieachse) eine vollständige Analyse durchgeführt werden.

"Light Rays in the Gravitational Field of Rotating Disks of Dust in General Relativity"

von Declan Moran

Zusammenfassung

Die bei weitem größte Informationsquelle, sowohl direkt als auch indirekt, die den Astrophysikern dieses Universums zur Verfügung steht, ist das Licht, welches uns aus den Fernen des Himmels erreicht. Auf seiner Reise wird dieses Licht von Gravitationsfeldern beeinflußt, die viel stärker sind, als jene, die wir von der Erde kennen. Je größer die Entfernung der Lichtquelle, desto wichtiger ist es, diese Gravitationseffekte zu berücksichtigen, nicht nur, weil solche Effekte zur Akkumulation neigen, sondern weil die größere Entfernung der Lichtquelle auch ein zeitliches Zurückgehen bedeutet, welches uns einen Blick in die Geschichte des Kosmos erlaubt. Einer der wichtigsten solcher Einflüsse auf diese Lichtstrahlen sind Galaxien, und die beste relativistische Beschreibung, die der Physik zur Verfügung steht, ist die Neugebauer-Meinel-Lösung der Einsteinschen Feldgleichungen. In erster Linie unter Verwendung dieser Lösung wurde der Einfluß der Gravitation auf Lichtstrahlen hinsichtlich drei verschiedener Aspekte untersucht.
Zuerst wurde das Bild der rotierenden Scheibe einschließlich der Rotverschiebung der beteiligten Photonen berechnet, was unter anderem veranschaulicht, wie extrem die Effekte eines starken Gravitationsfeldes auf Licht sein können. Besonders interessant ist die Tatsache, daß man, bedingt durch die Krümmung der Lichtstrahlen, gleichzeitig die Ober- und Unterseite der Scheibe betrachten kann. Für genügend große Werte des relativistischen Parameters μ ist es sogar möglich, mehrmals um die Scheibe zu sehen, mittels Lichtstrahlen höherer Ordnung. Die Verwendung passender Oberflächenstrukturen ermöglicht es dem Betrachter, die Effekte der endlichen Lichtgeschwindigkeit von denen zu trennen, die nur durch das Gravitationsfeld verursacht sind. Nachfolgende Untersuchungen konzentrierten sich auf einzelne Lichtstrahlen und die Berechnung ihres Ablenkwinkels. Hierzu wurden Formeln hergeleitet unter Verwendung der Kopeikin-Schäfer-Theorie der Lichtausbreitung für die radiale (nullte Ordnung) und die tangentiale Ablenkung (erste Ordnung). Außerdem wurden Vergleiche der Lösungen angestellt, die man bei Benutzung der Neugebauer-Meinel-Lösung bzw. der Ansorg-Meinel-Lösung erhält, die zeigten, bei welchem Wert des relativistischen Parameters μ man erwarten kann, daß die Annahme einer starren Rotation signifikant wird. Im dritten Teil wurde die Linsenstruktur der starr rotierenden Scheibe untersucht, besonders die kaustische Struktur. Solche Untersuchungen sind besonders nützlich zum Testen verschiedener Modelle der Standard-Linsentheorie (v.a. der elliptischen Linsenmodelle), die leider in ihrer Gültigkeit auf schwache Felder begrenzt sind. Die Nutzung der Neugebauer-Meinel-Lösung und direkte Integration der Geodätengleichungen ermöglicht es, diesen Näherungen und Begrenzungen auf schwache Felder zu entkommen. Sie erlauben einen Einblick auf extremere Gravitationslinsen und somit einen besseren Eindruck von dem Bereich, wo solche Modelle in der Standardtheorie von einer akurateren relativistischen Beschreibung, v.a. einschließlich der Rotationseffekte, abweichen.[1]

[1]In dieser Arbeit wird an verschiedenen Stellen der Begriff "Licht" verwendet, jedoch finden die anderen Formen elektromagnetischer Strahlung, einschließlich Radiowellen, in allen Ergebnissen und Überlegungen genauso Anwendung.